Applied Energy 408 (2026) 127424

Contents lists available at ScienceDirect

Applied Energy

journal homepage: www.elsevier.com/locate/apenergy

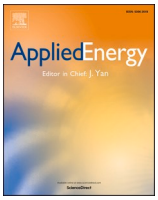

Synergistic operation and maintenance enabling lifecycle-aware opportunistic management of offshore wind energy

Jiaxin Zhang [a], You Dong [a,*], Dan M. Frangopol [b], Songye Zhu [a], Hongxing Yang [c]

[a] Department of Civil and Environmental Engineering, The Hong Kong Polytechnic University, Hong Kong 999077, China
[b] Department of Civil and Environmental Engineering, Engineering Research Center for Advanced Technology for Large Structural Systems (ATLSS Center), Lehigh University, Bethlehem, Pennsylvania, USA
[c] Renewable Energy Research Group (RERG), Department of Building Environment and Energy Engineering, The Hong Kong Polytechnic University, Hong Kong 999077, China

HIGHLIGHTS

- Develop an opportunistic operation and maintenance framework for offshore energy.
- Integrate structural control and maintenance scheduling under coupled wind-wave.
- Establish a DBN–POMDP model for lifecycle decision-making in dynamic environments.
- Propose a multi-attribute utility function covering cost, reliability, and sustainability.
- Apply deep reinforcement learning to optimize life-cycle O&M strategies.

GRAPHICAL ABSTRACT

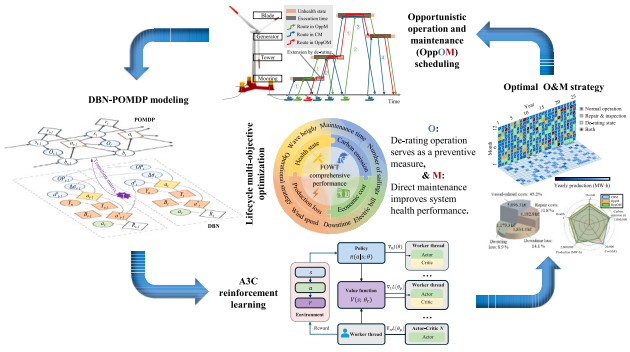

ARTICLE INFO

Keywords:
Opportunistic operation and maintenance
Multi-objective optimization
Integrated DBN-POMDP
Deep reinforcement learning
life-cycle analysis

ABSTRACT

Offshore wind power capitalizes on abundant wind resources and vast spatial availability, enabling a significant increase in turbine capacity. However, the deterioration of large-scale floating offshore wind turbines (FOWTs) under complex marine conditions remains a persistent challenge. Rapid structural degradation and the inaccessibility of far-offshore wind farms pose substantial hurdles to effective operation and maintenance (O&M) strategies. To address these challenges, an opportunistic operation and maintenance (OppOM) framework is proposed, integrating turbine de-rating control with maintenance scheduling to enable intelligent management over the lifecycle. The system state evolution of FOWTs under dynamic wind–wave environment is inferred using a Dynamic Bayesian Network (DBN). A Partially Observable Markov Decision Process (POMDP) then models the uncertainty in observations and guides decision-making through probabilistic reasoning. A multi-attribute utility function is developed to jointly consider turbine health, economic costs, energy yield, and carbon emissions as lifecycle O&M objectives. The integrated DBN-POMDP framework is ultimately solved using an Asynchronous Advantage Actor-Critic reinforcement learning approach. The proposed OppOM framework was benchmarked against conventional Condition-base maintenance (CBM) and de-rating free opportunistic maintenance (OppM). Compared to CBM, OppOM reduced total lifecycle costs by 30.4%. Relative to OppM, it achieved an 18.7% cost

* Corresponding author.
E-mail address: you.dong@polyu.edu.hk (Y. Dong).

https://doi.org/10.1016/j.apenergy.2026.127424
Received 13 August 2025; Received in revised form 15 November 2025; Accepted 16 January 2026
Available online 24 January 2026

reduction, 12.7% less downtime, and notable gains in energy output and CO_2 mitigation. Average system health index increased to 0.87, while component-level HI remained above 0.95 across the service life. The proposed OppOM framework establishes a new paradigm for offshore wind energy O&M by unifying structural control and maintenance planning. By incorporating turbine self-adaptive behavior into long-term governance, it enhances resilience to environmental uncertainty while improving lifecycle-level sustainability.

List of notations

Symbol / Acronym	Description
FOWT	Floating Offshore Wind Turbine.
O&M	Operation and Maintenance.
CM	Corrective Maintenance.
PM	Preventive Maintenance.
CBM	Condition-Based Maintenance.
OppM	Opportunistic Maintenance.
OppOM	Opportunistic Operation and Maintenance (joint planning of operation and maintenance actions).
DBN	Dynamic Bayesian Network.
MDP	Markov Decision Process.
POMDP	Partially Observable Markov Decision Process.
Pof	Probability of failure
RL	Reinforcement Learning.
A3C	Asynchronous Advantage Actor–Critic.
GA	Genetic Algorithm.
LSTM	Long Short-Term Memory network.
RNN	Recurrent Neural Network.
PPO	Proximal Policy Optimization.
DDPG	Deep Deterministic Policy Gradient.
POD	Probability of Detection (inspection detectability curve).
OPEX	Operating Expenditure.
LCOE	Levelized Cost of Energy.
$i \in 1,2,3,4$	Component index: 1 blade; 2 generator; 3 tower; 4 mooring.
$x_{i,t}$	Maintenance decision for component i at time t
y_t	Vessel mobilization at time t
dr_t	De-rating decision at time t; mutually exclusive with maintenance.
τ_t	Downtime duration on day t.
$z_{i,t}$	Indicator of repaired status used in the multi-attribute model.
$HI_{i,t}$	Health index of component i at time t.
$HI_i^{min}, HI_{sys}^{min}$	Component-level and system-level HI thresholds.
$E(t)$	Daily energy production accounting for downtime and efficiency.
$E_{dr}(t)$	Energy under de-rating; loss defined relative to nominal output.

1. Introduction

Floating Offshore Wind Turbines (FOWTs) are emerging as a critical pillar in the global energy transition, with deployment expanding rapidly due to their ability to access deeper waters and higher wind resources [1]. However, compared to onshore wind, offshore wind farms face much harsher operational and maintenance (O&M) challenges. The marine environment exposes turbines to more severe weather, salt corrosion, and complex sea states, while offshore logistics, such as transporting crews, vessels, and parts, become significantly more complicated and expensive [2]. Compared with bottom-fixed turbines typically deployed in near-shore waters, FOWTs face uniquely stringent coupled dynamics, mooring-specific fatigue risks, and offshore accessibility constraints. FOWTs exhibit strong aero-hydro-servo-elastic coupling, whereby platform motions interact with rotor aerodynamics and the generator–pitch loops, potentially introducing negative damping and non-minimum-phase behavior above rated [3,4]. Mooring fatigue and failure consequences are also more critical for floating concepts: waves dominate line-fatigue hotspots (including second-order and low-tension cycling), while single-line failure can induce significant platform drift and load redistribution that stresses remaining lines [5,6]. Finally, candidate floating sites are generally farther offshore and in harsher metocean regimes, which reduces accessibility and shortens viable O&M weather windows relative to existing fixed-bottom sites; comparative and techno-economic analyses indicate that downtime and O&M strategy become stronger at floating sites [7,8]. As a result, the O&M costs for offshore wind projects often account for as much as 20%–30% of the total lifecycle expenditure [9,10]. This high proportion underscores the urgent need for O&M strategies that are both cost-effective and capable of sustaining long-term, reliable operations [11]. To address these O&M challenges, the IEC TS 61400-28:2025 standard was recently released, emphasizing the importance of intelligent management of operation, maintenance, and inspections, and highlighting the necessity for risk-informed strategies [12]. Despite these advances, the standard mainly determines inspection frequency based on generic operational years, categorizing turbines into early, mid, and late stages. This approach does not leverage real-time health data for dynamic risk assessment or continuous update of O&M planning, making it difficult to adapt to the actual, changing conditions of individual turbines [12].

Traditional O&M strategies predominantly include Corrective Maintenance (CM) and Preventive Maintenance (PM), as shown in Fig. 1. CM is a reactive strategy where maintenance actions are only taken after a failure has occurred. While this approach appears to have low initial costs, in offshore wind scenarios, it leads to long downtimes and high emergency repair costs, especially when considering the harsh sea conditions and the logistical complexity of transporting repair teams and equipment to remote sites [13,14]. Furthermore, CM is particularly costly and inefficient for offshore wind farms, as sudden failures often require urgent intervention, lengthy transit times, and increased operational risk [15]. Although CM may be appropriate for non-critical components or failures that are difficult to predict, its negative impact on energy output and O&M cost makes it increasingly unsuitable for modern offshore operations [15,16].

To compensate for CM shortcomings, PM has been widely adopted. Preventive maintenance (PM) is a proactive approach where maintenance activities are scheduled based on historical data and manufacturer recommendations, following fixed time or operation intervals [2,17]. PM reduces the likelihood of unexpected breakdowns and prolongs component life by performing preventive interventions. However, its major limitation is rigidity: PM schedules may lead to unnecessary maintenance, driving up costs and downtime, as not all components deteriorate uniformly or require the same servicing frequency [18,19]. Additionally, PM lacks the ability to leverage real-time monitoring data to fine-tune maintenance timing, limiting its ability to guarantee optimal turbine performance [20]. A detailed analysis of PM strategies indicates that grouping maintenance tasks by component age can reduce repeat offshore trips and lower costs. However, excessively aggressive PM schedules may substantially increase labor and vessel expenses; one study reported a 166% rise in such costs despite a reduction in failure events [21]. Moreover, maintenance activities themselves carry the risk of inducing new faults.

To further overcome the deficiencies of CM and PM, Condition-Based Maintenance (CBM) has gained prominence. CBM uses predictive analytics to track the actual condition of turbine components, enabling maintenance actions to be performed precisely when needed, thereby reducing unnecessary interventions and extending equipment life [22,23]. The core of CBM lies in the integration of advanced sensor technologies, data acquisition systems, and intelligent algorithms to continuously track the health status of critical components [24]. When degradation or early warning signs are detected, targeted maintenance can be implemented before catastrophic failure, minimizing downtime and cost [24]. However, the current CBM paradigm is not without flaws. Most CBM maintenance actions are treated as isolated events and do not consider the overall complexity or opportunity for coordination in

offshore operations. More importantly, CBM frameworks often neglect the immense logistical costs associated with offshore interventions can represent over 70% of total O&M costs [25,26]. Fig. 2 underscores the critical financial impact of vessel operations and offshore logistics on the economic viability of FOWTs. Thus, minimizing the number of offshore trips and maximizing operational efficiency have become crucial focal points in the advancement of offshore wind O&M strategies [2,27].

Against this background, Opportunistic Maintenance (OppM) has emerged as a promising solution that integrates the strengths of CBM and PM while specifically targeting the high logistical costs of offshore operations [28,29]. Recent advances in OppM for offshore wind have established a more unified view of maintenance opportunities. McMorland et al. (2023) categorized OppM into internal and external triggers, emphasizing that curtailment or negative-price periods can be exploited as maintenance windows [11]:

- **Internal opportunities** arise when a turbine is already offline due to planned maintenance, unexpected faults, or performance degradation detected by CBM; these periods can be used to address additional maintenance needs on the same or nearby turbines, even if those components have not reached their scheduled maintenance intervals [20,30].
- **External opportunities** refer to favorable environmental windows, such as low wind speed or calm seas, when the cost of downtime is low, allowing for maintenance actions with minimal impact on power production [24,25]. Early research (e.g., Besnard et al. [31]) demonstrated that leveraging such external opportunities can significantly reduce O&M costs, and follow-up studies have confirmed substantial cost savings [32].

Building on this foundation, Si et al. proposed a holistic scheduling and routing framework for offshore wind farms [33], while Li et al. formulated a multi-objective O&M optimization model under uncertainty [34]. Together, these studies define the current frontier of opportunity-aware O&M under harsh marine conditions, forming the

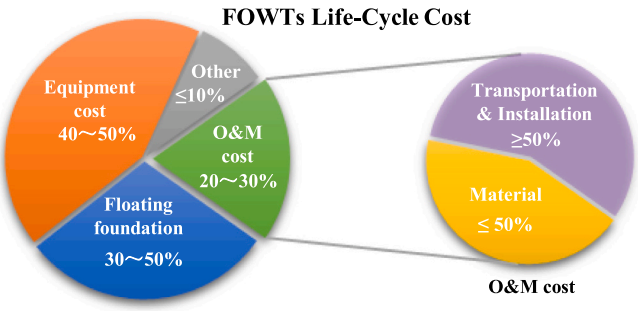

Fig. 2. Cost distribution of offshore wind turbine maintenance.

baseline upon which the present study extends to the floating offshore domain. Parallel progress in predictive maintenance has strengthened the information backbone of modern O&M. Xiang et al. demonstrated a deep-learning approach for wind turbine condition monitoring and anomaly detection [35], and Lee et al. incorporated deep reinforcement learning into maintenance scheduling [36]. The studies highlight the growing maturity of prognostics for offshore turbines; nevertheless, most frameworks still rely on deterministic scheduling and overlook uncertainty in health assessment and accessibility. Addressing this challenge, the present study advances predictive work toward a probabilistic decision framework capable of optimizing maintenance timing under partial observability and varying offshore conditions. For FOWTs, O&M continues to dominate lifecycle performance and cost. Centeno-Telleria et al. showed through techno-economic and comparative analyses that accessibility and heavy-maintenance strategies crucially affect economic viability [7,37]. The insights underscore the importance of maintenance models that explicitly value weather and accessibility constraints.

Most research on OppM focuses on optimizing the deployment of vessels, crews, and spare parts using advanced scheduling algorithms to maximize the benefit from both internal and external opportunities,

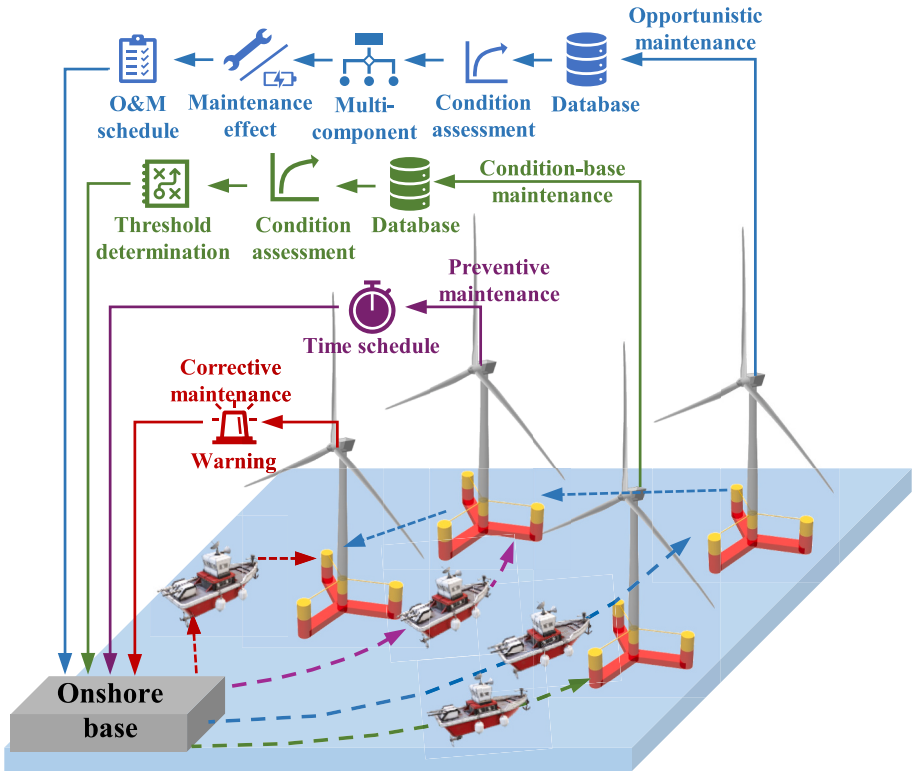

Fig. 1. Main maintenance approaches for offshore wind turbines.

reducing total O&M expenditure and enhancing resource efficiency [28,29,38,39]. Despite these advantages, effective OppM requires complex real-time decision-making frameworks that must handle multiple, often conflicting objectives: minimizing cost, maximizing energy yield, and guaranteeing equipment reliability [40–42]. Recent studies have begun to explore the use of deep reinforcement learning and other advanced AI techniques to meet these challenges [43,44].

Traditional methods such as Markov Decision Processes (MDP) and Genetic Algorithms (GA) have been applied to maintenance optimization in wind farms and related infrastructure domains, but they face fundamental limitations with high-dimensional state spaces, complex system interdependencies, and slow response to dynamic operational data [45–47]. In structural maintenance, for example, most work focuses on individual components using periodic inspections and life prediction models, but optimizing resource allocation and safety assessment across networks remains a significant challenge [48,49].

Recent years have witnessed a surge in the application of deep learning methods (such as LSTM and RNN) for health state prediction [50–52], but these approaches still struggle with generalization and real-time adaptation in complex, data-scarce environments. Recent years have seen Reinforcement learning (RL) emerge as a breakthrough technology in the O&M of wind farms, particularly for large-scale, offshore applications [53]. For instance, Arcieri et al. employed a PPO-based RL model for multi-maintenance team scheduling in a 50-turbine scenario, leading to significant improvements in O&M efficiency compared to rule-based dispatching [54]. Zhou et al. developed an RL controller based on load feedback that reduced turbine fatigue loads by 15% [55]; Pinciroli introduced an RL strategy to implement fault-tolerant control while optimizing power and frequency responses [56]; and Wu et al. employed multi-agent DDPG for yaw control, resulting in an 8.7% increase in power generation [57]. In the domain of predictive and CBM, Saleh et al. integrated RL with Petri net modeling to dynamically sequence and group maintenance tasks, achieving up to 99.4% simulated turbine availability [58]. Further, multi-agent RL frameworks such as the AGA-DDPG approach have been developed to support collaborative decision-making for edge-computing-enabled maintenance task allocation, substantially reducing computational burden in high-load scenarios [59]. Valet et al. presented a deep RL method for opportunistic maintenance scheduling, which integrates real-time component health, weather, and logistics to minimize offshore trips and total O&M cost, outperforming traditional heuristics in asset availability and operational efficiency [43]. Comprehensive reviews such as Oh et al. highlight RL unique strengths in adaptive inspection planning, resource allocation, and predictive maintenance for large, distributed wind farms, emphasizing its critical role in scaling up digital and autonomous O&M strategies [23]. It is worth noting that RL-based O&M approaches are increasingly providing an integrated "perception–decision–control" loop for wind energy systems. By leveraging real-time health data and operational feedback, these frameworks can dynamically adjust inspection, maintenance, and logistics decisions, supporting proactive asset management and optimized resource deployment even in highly uncertain offshore environments.

Despite this progress, most O&M research has largely neglected the fundamental role of turbine control strategies in affecting component fatigue and subsequent maintenance needs [60,61]. Beyond maintenance, current control strategies act as "soft" interventions that reshape structural loading and fatigue trajectories over the turbine's lifetime. In practice, collective blade-pitch and generator-torque control reduce cyclic stresses on blades and towers and suppress resonant responses, while active tower-damping controllers counter structural modes to further curb oscillation amplitudes and fatigue demands [62,63]. For floating turbines, modified pitch/torque laws are essential to avoid negative-damping instabilities, reducing platform pitch motion and mooring-line fatigue with minimal energy penalty [64]. Under high winds or strong turbulence, power de-rating (DR) limits thrust and shock loads and prevents over-stress of rotors and substructures; quantitative studies report 2–6% fatigue reductions at low winds and up to 6.5% tower fore-aft fatigue reduction in follow-on work [65,66], ultimate-load drops of ~31% (blades) and ~21.7% (towers) and 3–8.9% decreases in fatigue-equivalent loads [67], as well as up to 57.1% fatigue reduction via optimized DR and 10.7%/36.2% dynamic-load cuts on blades/towers, respectively [68,69]. When real-time damage assessment is embedded into the control loop, damage accumulation can drop by ~40% [70], and pairing with SHM-guided set-point optimization enables earlier intervention and longer maintenance intervals without sacrificing farm-level efficiency [71,72]. However, de-rating curtails energy output [73], making explicit the lifecycle trade-off among energy yield, structural reliability, and O&M cost. Despite the advances, most O&M studies still treat control exogenously and may overlook how poor tuning amplifies loads, especially in FOWTs with strong aero-hydro-servo coupling [74–76]. The gap motivates our work: jointly optimize control (notably DR) and opportunistic maintenance so that short-term load mitigation translates into long-term reliability gains and lower lifecycle O&M, rather than being handled in isolation [70,76,77]. Related cross-domain joint studies that co-optimize control with OppM further reinforce the value of a lifecycle-aware approach [78].

In summary, current research often focuses on external interventions, while insufficiently addressing the interplay between internal control strategies and O&M needs over the lifecycle. For FOWTs, bridging this gap is both scientifically important and practically urgent. Therefore, this research aims to establish a novel paradigm for FOWT O&M that systematically coordinates internal control actions (notably DR) with external maintenance activities, as shown in Fig. 3, leveraging RL reinforcement learning for dynamic, data-driven optimization. A three-layer synergistic innovation for FOWT operation and maintenance is proposed in this study:

(i) De-rating control is incorporated as an active load mitigation mechanism and jointly modeled with opportunistic operation and maintenance (OppOM), enabling coordination between operational control and maintenance decisions.

(ii) A unified framework combines dynamic Bayesian network (DBN) for online health belief updating with a partially observable Markov decision process (POMDP) that determines optimal "control + maintenance" policies.

(iii) The model integrates health, cost, power generation, and carbon factors into a multi-attribute utility function and employs the A3C deep reinforcement learning algorithm to solve high-dimensional decision problems efficiently.

The structure of this paper is organized as follows: Section 2 introduces a DBN integrated with a POMDP to enable efficient inference of

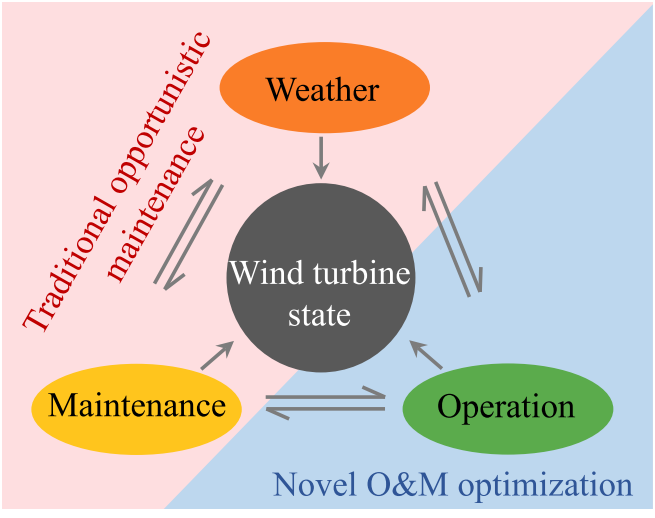

Fig. 3. A novel integrated operation and maintenance strategy.

FOWT degradation under stochastic wind and wave conditions. Section 3 presents the concept of OppOM and establishes its mathematical formulation. Section 4 formulates a multi-objective O&M optimization framework for FOWTs, incorporating safety, economic cost, energy yield, and carbon emissions as lifecycle performance objectives. This section also details the RL-based approach adopted to solve the optimization problem. Section 5 presents the results and key findings. Finally, Section 6 summarizes the main conclusions and outlines future research directions. Throughout, O&M is handled on a lifecycle basis: DBN belief is propagated over the 25-year horizon into a POMDP for long-horizon control–maintenance coupling; time-varying DR modifies transitions and fatigue; and a multi-attribute utility unifies health, energy, cost, and carbon.

2. Degradation of FOWT under dynamic environment

2.1. Hybrid DBN model for damage propagation modeling

FOWTs are exposed to multiple environmental loads, including wind, waves, and ocean currents, which contribute cumulatively to structural degradation over time. Therefore, accurately modeling their failure behavior requires explicit consideration of these degradation mechanisms [29]. The deterioration process is primarily driven by the accumulation of external dynamic loads and progressive internal material aging [79]. While existing machine learning models such as Long Short-Term Memory (LSTM) networks have shown promise in predicting short-term structural responses [80], they remain inadequate in capturing long-term degradation in system health. In contrast, DBNs, as a class of probabilistic graphical models with temporal inference capabilities, provide a rigorous framework for reasoning about long-term performance [81]. Methodologically, Morato et al. demonstrated that integrating DBNs with POMDPs yields more cost-effective policies than heuristic rules when asset health is uncertain [82]. Building upon this foundation, in this study, DBNs are adopted to analyze the degradation behavior of FOWTs under stochastic wind and wave environments.

The long-term performance degradation of structures typically involves both time-dependent and environment-dependent factors [83,84]. Although the mechanical–environmental interaction is not modelled explicitly, previous studies have demonstrated that the additive representation remains a reliable and widely adopted approximation in engineering applications, without compromising the fidelity of lifecycle degradation predictions [85]. The time-dependent degradation is often characterized using statistical methods based on historical data and underlying physical mechanisms. In this study, the degradation process is modeled using a Weibull distribution [86]. This section presents a comprehensive description of the integrated degradation model and decision-making framework developed in this study. Specifically, the framework consists of the following logical layers: firstly, environmental effects on structural degradation are quantified through stress-history analysis of wind, wave, and current loads; secondly, individual degradation sub-models are constructed by inputting stress histories into the Weibull natural degradation model and the Paris crack growth model, respectively; subsequently, these two distinct degradation mechanisms are integrated into a unified probabilistic degradation model using DBN.

The statistical behavior of natural degradation can be described using its probability density function and corresponding rate, which are expressed as follows:

$$f(t;\alpha,\beta)=\frac{\beta}{\alpha}\left(\frac{t}{\alpha}\right)^{\beta-1}\exp\left[-\left(\frac{t}{\alpha}\right)^{\beta}\right],\lambda(t)=\frac{\beta}{\alpha}\left(\frac{t}{\alpha}\right)^{\beta-1} \tag{1}$$

where α denotes the scale parameter, representing the characteristic lifetime, and β is the shape parameter, dictating the trend of the degradation rate. The degradation parameters of the four critical components of FOWT are shown in Table 1.

Table 1
Time-dependent degradation model parameters [28].

Component	Annual failure rate	Functional failure
Blade	0.0348	α=1.2, β=2.88
Generator	0.052	α=1.2, β=1.92
Tower	0.067	α=1.2, β=14.93
Mooring	0.006	α=1.2, β=16.67

Furthermore, fatigue crack growth is a critical contributor to the long-term degradation and eventual failure of offshore structures. To model this process under wind and wave loading, the Paris law is adopted, which is widely recognized for characterizing the rate of crack length propagation per stress cycle [87]. Utilizing measured data, this study applies spectral analysis and the Rainflow Counting Method to extract the number of stress cycles n_i and corresponding stress ranges $\Delta\sigma i$ [88]. The governing equation of crack development is given by:

$$\frac{da}{dN}=C(\Delta K)^m \tag{2}$$

where a is crack length, N represents stress cycle count, and parameters C and m, represent crack growth rate and material sensitivity to loading, respectively. The C and m values for different component materials are shown in Table 2.

The stress intensity factor range ΔK directly correlates with the stress history, reflecting the stress concentration at the crack tip [1].

$$\Delta K=Y\Delta\sigma\sqrt{\pi a} \tag{3}$$

where geometric factor Y depends on crack location and structural geometry, determined through finite element analysis or experimental data.

Integrating and discretizing Paris' law probabilistically yields the transition probability from crack length state a_i to a_j:

$$P(a_{t+1}=a_j|a_t=a_i)=\int_{a_j}^{a_{j+1}}f(a|a_i,\Delta\sigma)da \tag{4}$$

In this study, DBNs are adopted to jointly represent natural degradation and fatigue crack propagation in structural components. By incorporating both physical degradation models and observational data, the framework enables dynamic inference of structural health over time. Fig. 4 presents the DBN-based analytical framework used to model crack growth in offshore structural components under stochastic environmental loading.

where m_t and m_{t-1} are static nodes representing the material crack growth exponent, and $\Delta\sigma_t$ and $\Delta\sigma_{t-1}$ denote the stress range applied to the structure at each time step. The variables a_t^0 and a_{t-1}^0 are the prior crack length distributions before inspection or repair, where a_t and a_{t-1} are the crack lengths updated via Paris' law. The nodes Y_t and Y_{t-1} represent the observed information, and Y_n denotes the system noise and observation uncertainty. The observed nodes B_t and B_{t-1} capture the inspection outcomes. The variables a_t^* and a_{t-1}^* are the posterior crack lengths after applying inspection and repair decisions, where a_r is the repair crack length distribution representing the restored condition. Finally, R_t and R_{t-1} are functional nodes based on the crack length and a defined failure threshold.

The system state at time t is defined as:

Table 2
Paris-law parameters C, m by component

Component	C	m
Blade [89]	6.16×10^{-8}	5.4
Generator [90]	2.70×10^{-11}	2.88
Tower [90]	2.70×10^{-11}	2.88
Mooring [90]	3.46×10^{-8}	1.11

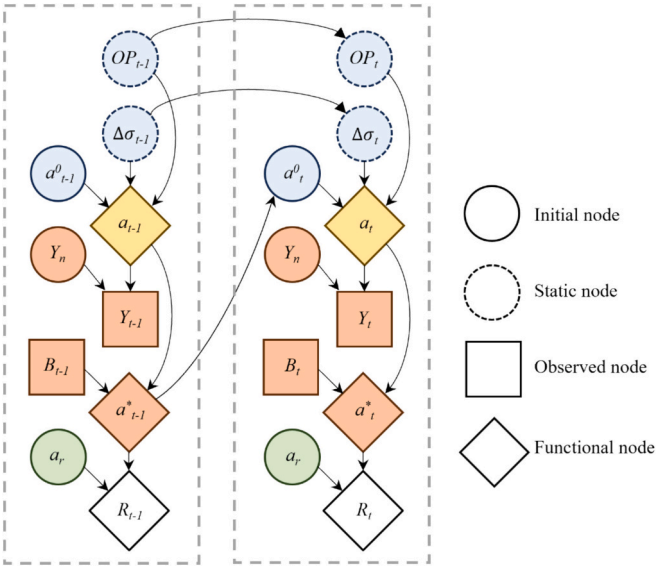

Fig. 4. DBN-based analytical framework for crack propagation in structural components.

$$S_t = (d_t, a_t) \tag{5}$$

where d_t denotes the natural degradation state modeled by the Weibull distribution; a_t represents the crack length state modeled by the Paris crack growth model.

The state transition dynamics are encoded using conditional probability tables [91], assuming independence between natural degradation and crack growth mechanisms:

$$P(S_{t+1}|S_t) = P(d_{t+1}|d_t, \alpha, \beta)\cdot P(a_{t+1}|a_t, \Delta\sigma) \tag{6}$$

The main focus of this study is to establish an integrated O&M optimisation framework that simultaneously considers multiple turbine subsystems and incorporates de-rating control into the maintenance decision space. This system-level integration represents the core methodological contribution. While more advanced deterioration models exist, such as corrosion–fatigue formulations require non-stationary and regime-switching state transitions, which are not directly compatible with the DBN-POMDP structure adopted here. Under the site conditions considered in this work, the adopted model and a corrosion–fatigue model exhibit only minor differences during the period in which maintenance interventions are expected to be triggered. Appendix A further shows that the potential acceleration in later stages would be suppressed in practice. Therefore, the adopted crack-growth model is suitable for the purpose of evaluating the O&M strategy.

Inspection results are integrated into the DBN via observation nodes O_t, modeled using Probability of Detection (POD) curves [92]:

$$PoD(O_t = o|a_t) = \frac{1}{1 + (X_0/a_t)^b} \tag{7}$$

where $X_0$and $b$represent characteristic inspection parameters, calibrated from controlled hit trials or field inspections; specifically, X_0 equals the 50% detection size a_{50} and b governs the transition steepness, with the 90% detection size obtained as $a_{90} = X_0\, 9^{1/b}$under the adopted modality- and component-specific flaw-size definition. The parameters in this study were derived from engineering-like test data [93–95], and the specific values are listed in Table 3.

Table 3
Component-wise PoD parameters and implied detection sizes

Component	Adopted (X_0, b)	Implied points
Blades [95]	X_0=2.70, b=2.05	a_{50}=2.70 mm; a_{90}=7.90 mm
Generator [93]	X_0=5.30, b=3.26	a_{50}=5.30 mm; a_{90}=10.4 mm
Tower [93]	X_0=1.81, b=5.5	a_{50}=1.81 mm; a_{90}=2.7 mm
Mooring [94]	X_0=9.62, b=3.0	a_{50}=9.62 mm; a_{90}=20.0 mm

Through Bayesian updating within the DBN framework, observational data updates the state probability distributions effectively. The updating procedure includes:

1) Forward propagation (prediction step): Predicting future state distributions based on current probabilities and transition probabilities.
2) Backward updating (correction step): refining those predictions based on new observational evidence.

2.2. Integrated POMDP-DBN for FOWT modeling

DBNs are employed to model structural deterioration processes and to update uncertainty based on observational data. However, they lack intrinsic optimization capabilities, making them insufficient for deriving optimal decision strategies. To address this limitation, DBNs are integrated with Partially Observable Markov Decision Processes (POMDPs), which enable sequential decision-making under uncertainty [82]. This section demonstrates how the combined framework leverages dynamically updated belief states to formulate optimal inspection and maintenance policies that minimize life-cycle costs under partial observability. The POMDP offers a rigorous decision-optimization framework tailored for environments characterized by uncertainty and partial observability. In the context of FOWTs, where component degradation states are not directly measurable and both environmental loading and degradation dynamics exhibit intrinsic stochasticity, the POMDP is utilized to adaptively optimize O&M over time [96]. Within this framework, the probabilistic degradation and observation models derived from the DBN are embedded into the POMDP structure, establishing a closed-loop, data-informed decision-feedback system, as illustrated in Fig. 6. Inputs from degradation models (failure probabilities, crack growth data, observation results) are processed through the DBN to estimate state transition probabilities. The POMDP layer then determines optimal actions (repair, inspection, or DR) under uncertainty. The resulting reliability indices and decision policies are passed as inputs to the OppOM framework in Section 3.

The POMDP model is formally defined as the tuple $\langle S, A, \Theta, \boldsymbol{T}, \boldsymbol{O}, \boldsymbol{R}, \gamma\rangle$, where:

- S denotes the system state space, specified as $S_t = (d_t, a_t)$, with d_t representing the underlying environmental degradation state and a_t denoting the measurable structural damage.
- A defines the discrete action space, including “Do Nothing” (DN), “Repair” (RP), and “De-rating” (DR). RP in OppOM admits two trigger modes: opportunistic (scheduled under external windows, e.g., low wind/wave, or internal windows when another component is already scheduled, allowing pre-threshold, parallel repairs) and reactive (scheduled once a component crosses its health threshold). The DR action directly alters the state transition matrix. In contrast, the RP action resets the structural state by restoring damaged components to a healthier condition. The effects of these actions on system evolution are detailed in Fig. 5.

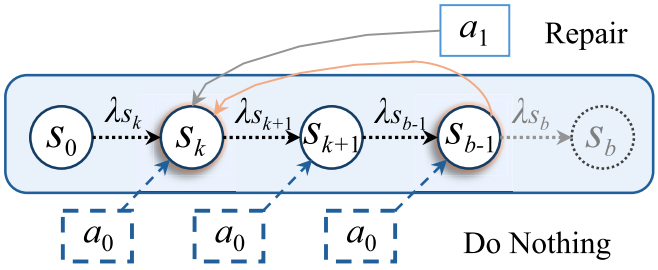

Fig. 5. MDP showing repair actions taken for components.

- $O = \{o_D, o_{ND}, o_0\}$ defines the observation space, where o_D corresponds to a crack detection event, o_{ND} indicates a non-detection outcome, and o_0 represents the case in which no observation is conducted.
- $T(s'|s,a) = P(S_{t+1} = s'|S_t = s, a_t = a)$ is the state transition model provided by DBN. Within each time step, the joint transition factorizes as $T(S_{t+1}|S_t) = T_d(d_{t+1}|d_t;\alpha,\beta)\,T_a(a_{t+1}|a_t,\Delta\sigma;C,m)$, inspections contribute via the POD-based likelihood $Z(o_t|a_t;X_0,b)$, enabling Bayesian filtering of the coupled degradation state.
- $Z(o|s,a)$ is the observation model, the model is parameterized using the POD curve, where *PoD* is defined in Eq. 7.

$$Z(os,a) = \begin{cases} PoD(a_t), & a = IM, o = o_D \\ 1 - PoD(a_t), & a = IM, o = o_{ND} \\ 1, & a = DN, o = o_0 \\ 0, & Otherwise \end{cases} \tag{8}$$

- $R(s,a)$ is the reward function. In this study, the multi-attribute utility formulation described in Section 4.1 is directly used as the reward model.

Since the true system state is not directly observable, the POMDP

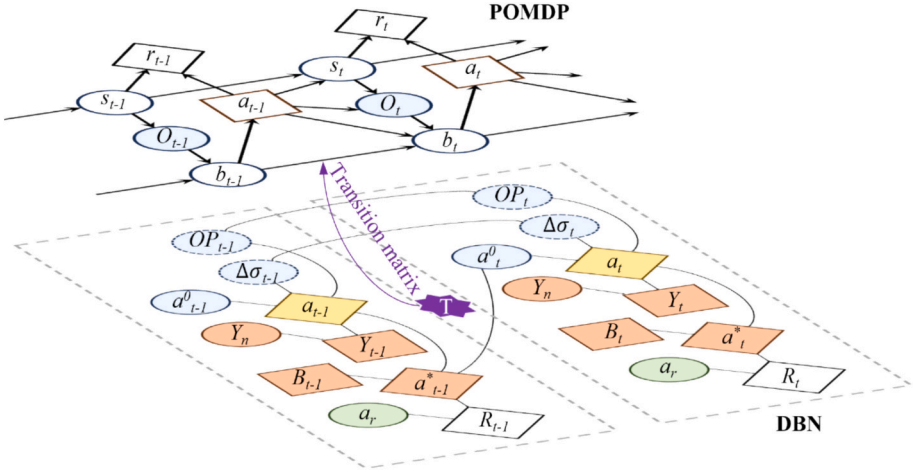

Fig. 6. Integrated DBN–POMDP decision-making framework for FOWTs.

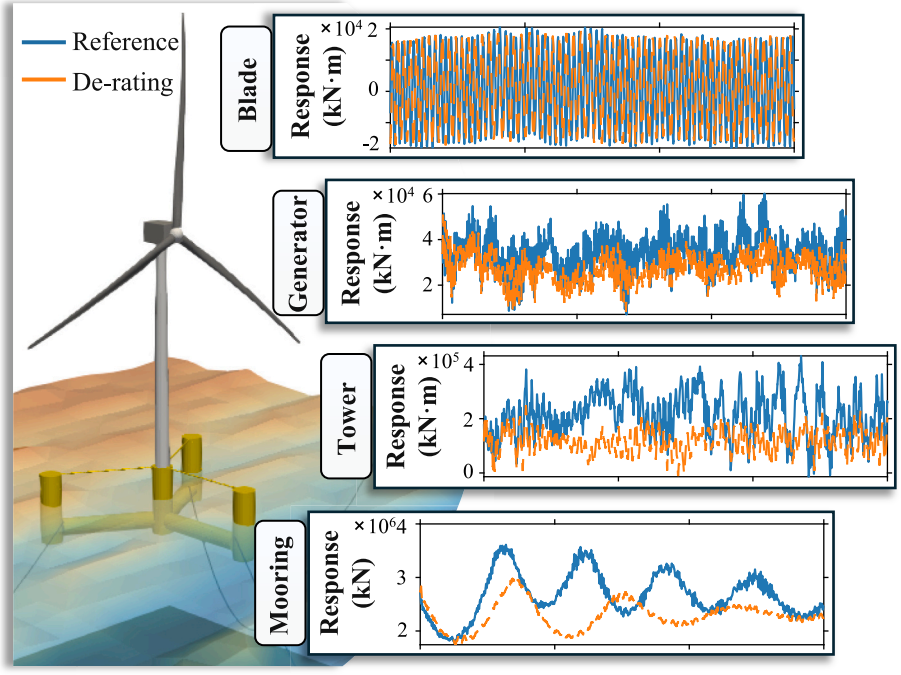

Fig. 7. Comparative structural response under the DR strategy, illustrated using a representative case with a mean wind speed of 15 m/s.

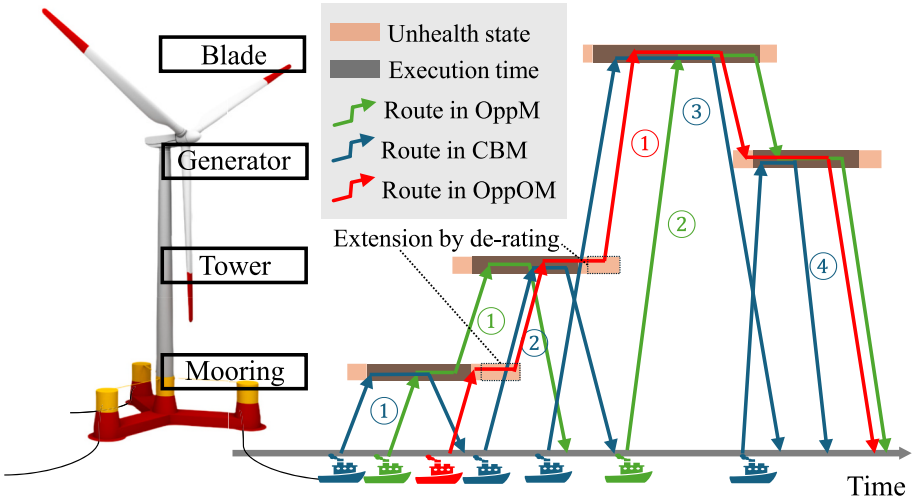

Fig. 8. Concept of opportunistic operation and maintenance (OppOM).

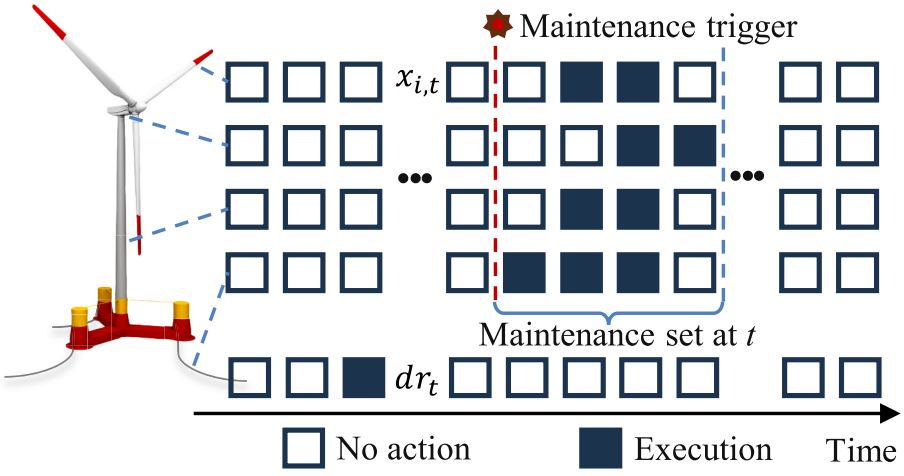

Fig. 9. The schematic diagram of O&M action variables in OppOM.

framework maintains a belief state $b_t(s)$, representing a probability distribution over possible states. Upon executing action a_t and receiving observation o_{t+1}, the belief is updated according to:

$$b_{t+1}(s') = \tau(b_t, a_t, o_{t+1}) = \eta Z(o_{t+1}|s', a_t) \sum_{s \in S} T(s'|s, a_t) b_t(s) \tag{9}$$

where η is a normalization constant ensuring $b_{t+1}(s')$ sums to one. The transition and observation models T and Z are derived from the DBN, enabling tight integration between probabilistic modeling and decision optimization.

To solve the POMDP, this study adopts point-based solution methods suitable for high-dimensional belief spaces [97]. These methods approximate the value function $V(b)$ over selected belief points:

$$V(b) = \max_{a \in A} \left[\sum_{s \in S} b(s) R(s, a) + \gamma \sum_{o \in O} P(o|b, a) V(b') \right] \tag{10}$$

where b' is the updated belief state after taking action a and observing o.

The optimal policy $\pi^*(b)$ is derived as:

$$\pi^*(b) = \operatorname{argmax}_{a \in A} \left[\sum_{s \in S} b(s) R(s, a) + \gamma \sum_{o \in O} P(o|b, a) V(b') \right] \tag{11}$$

In summary, the POMDP-based decision-making framework integrates probabilistic inference from the DBN to continuously update the belief state and inform optimal inspection and maintenance decisions under uncertainty. The degradation modeling framework developed in this section establishes a probabilistic foundation for describing the health evolution of key FOWT components. The outputs from the DBN–POMDP—specifically, the health indices, degradation states, and optimal actions represent the essential inputs for higher-level lifecycle planning. However, degradation modeling alone cannot fully exploit the coupling between structural deterioration and operational control strategies such as DR. To bridge this gap, the following section introduces the concept of OppOM, which extends the DBN–POMDP results toward a lifecycle-aware framework that jointly optimizes repair scheduling and power control decisions.

3. Lifecycle-aware opportunistic O&M (OppOM)

3.1. Concept of OppOM

Maintenance actions for wind turbines are generally aimed at improving performance and ensuring operational efficiency throughout the entire life cycle. Lifecycle awareness in wind energy denotes an end-to-life capability that maintains a continuously updated health belief from environment–degradation–observation–action data, optimizes coupled control–maintenance under partial observability for long-horizon returns, actively reshapes degradation via operational levers,

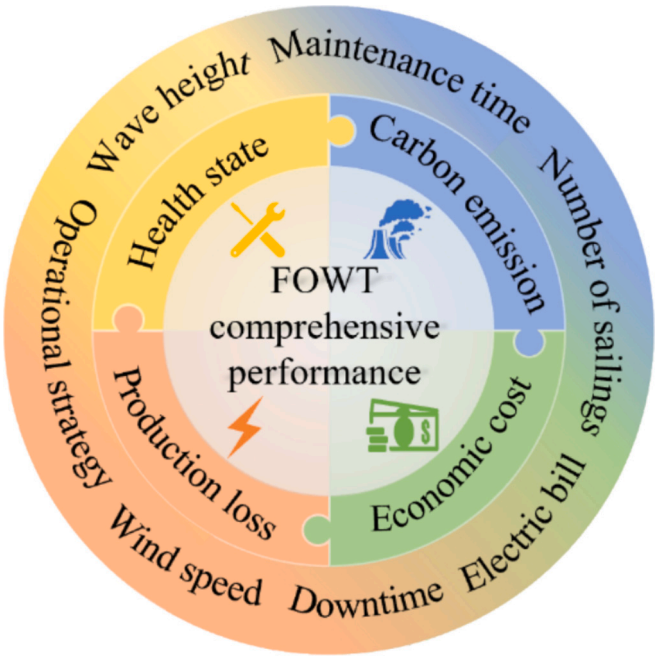

Fig. 10. Multi-attribute function on FOWT.

and evaluates decisions on a unified multi-attribute utility over reliability, energy, cost, and carbon. Due to the complex and harsh offshore environment, observation and actions often rely on specialized vessels, which significantly limits their timeliness and accuracy [21,98]. As detailed in the Introduction, the prevailing state-of-the-art approach is the OppM strategy, which optimizes maintenance efficiency by capitalizing on planned downtimes or scheduled maintenance events to address additional repair needs [33,99]. By tackling multiple issues while the turbine is already offline, this method reduces the frequency of maintenance visits, lowers overall costs, and minimizes downtime, thereby enhancing both the efficiency and reliability of offshore wind operations [100]. However, such strategies typically overlook the potential of control-based approaches in actively mitigating structural loads and delaying degradation through turbine-side intervention [101]. As illustrated in Fig. 7, compared to a baseline 15 MW FOWT operating under the reference controller [102], the implementation of a DR control strategy (with a reduced rated wind speed of 7 m/s [103]) results in significantly attenuated structural dynamic responses. This further validates the effectiveness of integrating DR as a preventive mechanism within the broader O&M framework for FOWTs.

Unlike conventional maintenance actions that are discrete and reactive, DR functions as a long-term, continuous intervention, with its cost directly tied to real-time energy yield reduction rather than upfront capital or service expenses. This necessitates dedicated modeling and integration of DR within the overall O&M optimization framework.

From a practical standpoint, DR offers several distinctive advantages:

1) Higher cost-effectiveness: it enables structural performance improvements without physical intervention, reducing reliance on high-cost marine logistics [73,98].

2) Operational flexibility: it can substitute for physical repairs during periods when on-site access is limited or infeasible, while aligning with favorable weather/low-wind windows and harsh sea states [64,104].

3) Global degradation mitigation: as a system-level strategy, DR has the potential to simultaneously and proportionally reduce degradation rates across multiple components [66,67] , thereby extending the overall lifespan.

Collectively, these features position DR not merely as a backup control option, but as a strategic element in next-generation lifecycle-aware O&M frameworks for FOWTs.

3.2. *Collaborative synergies of operation and maintenance*

The dynamic coupling between structural degradation and operational control in offshore wind turbines necessitates an integrated approach to lifecycle management. As established in Section 3.1, turbine control strategies have a pronounced effect on structural responses, which in turn influence damage accumulation in critical components. This interdependence exposes a fundamental limitation in conventional O&M strategies, which typically treat maintenance planning and power generation as separate domains. Building on this insight, the OppOM framework is introduced to strategically integrate DR actions with conventional maintenance scheduling. Rather than treating operational control and structural maintenance as independent domains, OppOM leverages their dynamic coupling to reshape degradation trajectories and create synchronization windows for maintenance execution. The OppOM framework leverages the degradation states and reliability information derived from the DBN–POMDP to co-optimize repair grouping and operational DR strategies.

As illustrated in Fig. 8, the blue lines denote CBM-derived triggers

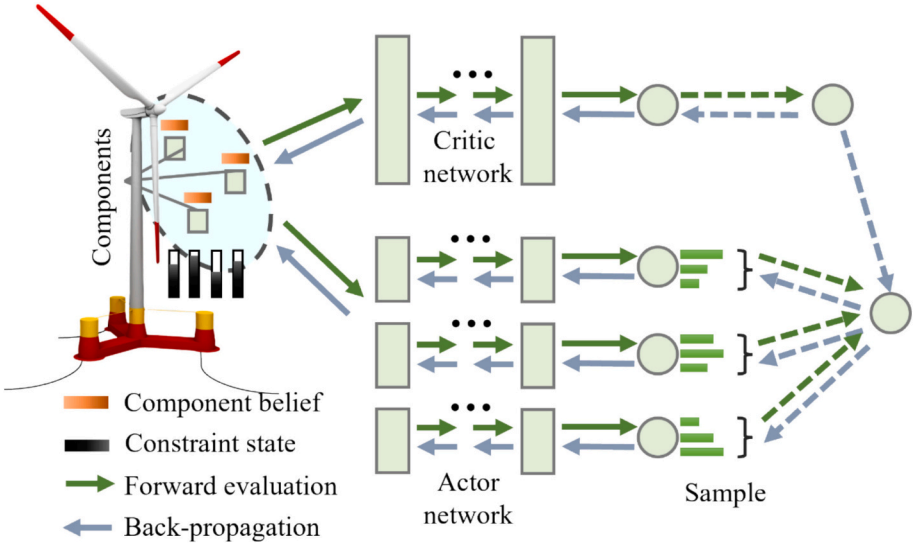

Fig. 11. The architecture of AC neural networks on multi-component FOWT.

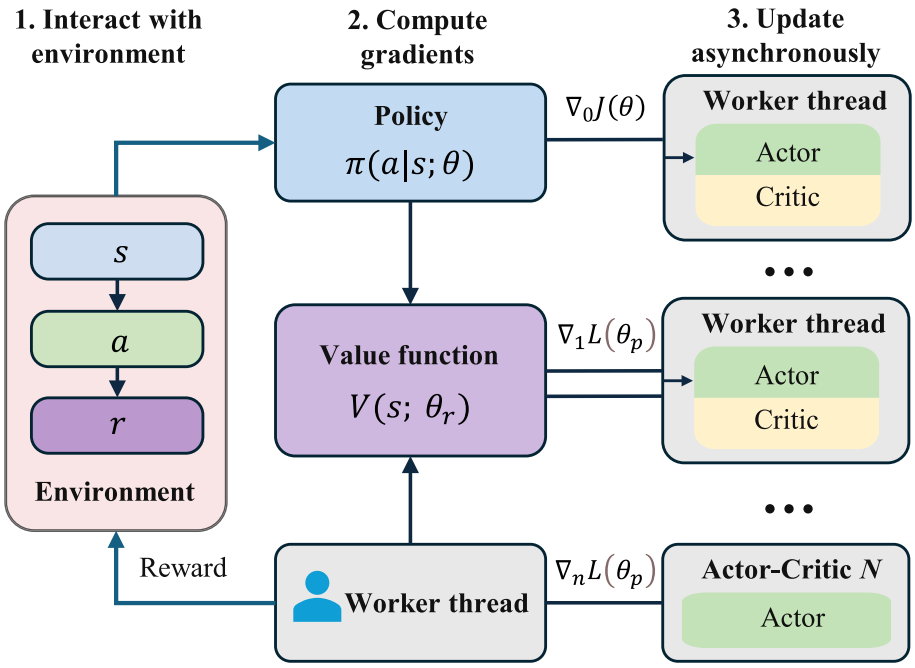

Fig. 12. Asynchronous Actor-Critic framework architecture.

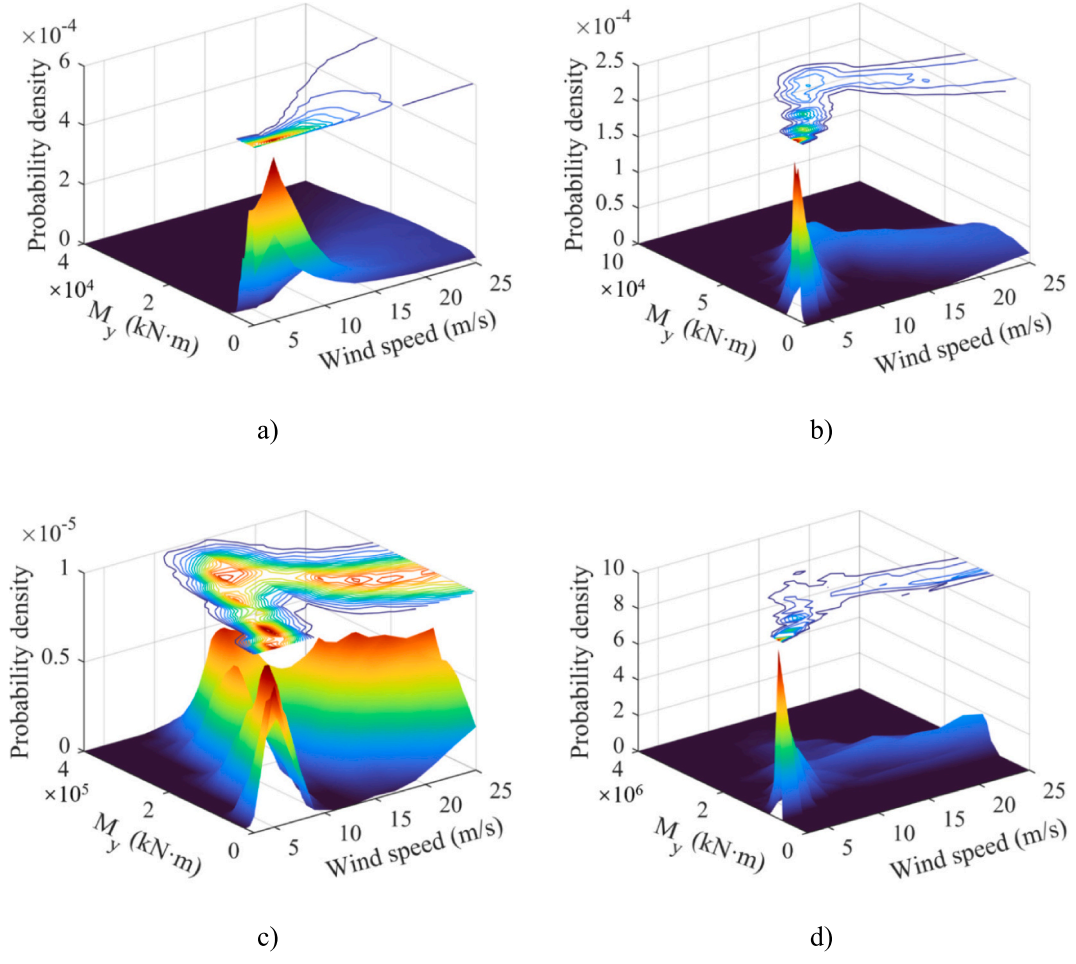

Fig. 13. Stress distribution under different wind speed of multi-component. a) Blade; b) Generator; c) Tower; d) Mooring.

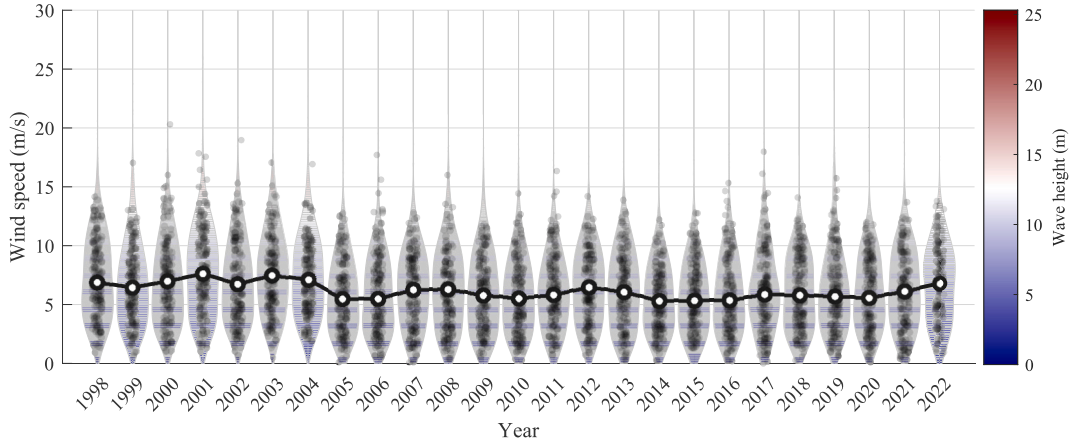

Fig. 14. Wind speed distribution over 25 years in the selected analysis region.

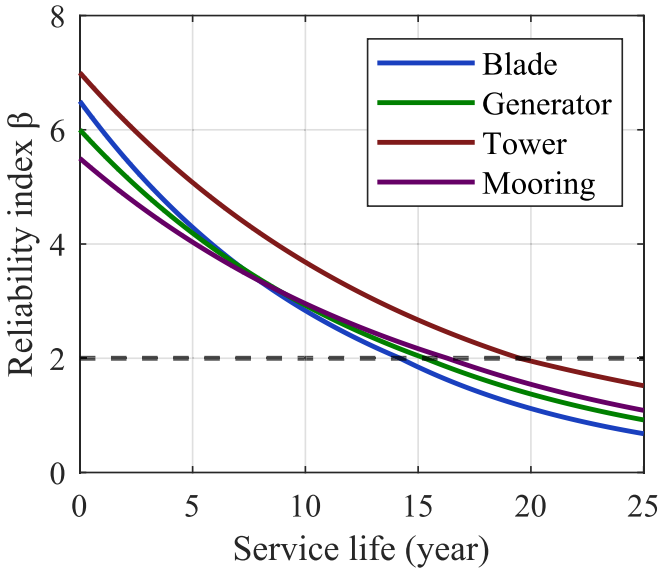

Fig. 15. Reliability development of each component

and actionable windows, the green trajectory shows the route under OppM without control coordination, and the red trajectory shows the route under OppOM. Light-orange bars mark "unhealthy but tolerable" windows and gray segments indicate repair execution time. The purple dashed blocks ("Extension by DR") represent the additional deferrable window created after a trigger by temporarily DR the turbine: during this interval the unit continues to operate at reduced power while degradation is slowed, effectively shifting the right boundary of the actionable window; the extension is bounded by structural-health and maximum-deferral constraints and terminates at the consolidated outage.

Under OppM, tasks can only be bundled when these fixed CBM windows happen to overlap, which often yields multiple routes. OppOM treats DR as a control decision to reshape windows, safely lengthening the earlier one until it intersects the later one, thereby consolidating tasks into a single shared outage. Economically, the framework is justified by two compensatory mechanisms: (1) reduced cumulative production loss by clustering maintenance events into shared outages, and (2) extended deferrable maintenance windows enabled by controlled degradation pacing. DR is a preventive operational action (rather than a physical maintenance task) that does not rely on site accessibility, thus increasing operational flexibility under constrained access conditions. Consequently, the OppOM framework jointly optimizes turbine control and maintenance execution, increasing the likelihood of synchronizing multiple actions under a shared trigger while respecting structural-health limits and reducing overall life-cycle costs.

The contribution of this work lies in a unified O&M decision framework that jointly optimises de-rating and maintenance under partial observability. Because the emphasis is on decision coupling rather than exhaustive physics of any single sub-process literature-supported assumptions is adopted to keep the problem solvable. The points of use and justification are consolidated in Table 4.

The FOWT in OppOM is modeled as a system comprising four critical structural components, indexed by $i \in \{1, 2, 3, 4\}$, representing the blade (1), nacelle (2), tower (3), and mooring system (4). The planning horizon is discretized into daily time steps, denoted by $t \in \{0, 1, 2, \ldots, T\}$. A binary decision variable $x_{i,t}$ is defined to represent whether a repair action is scheduled for component i at time step t, where $x_{i,t} = 1$ indicates that the repair is performed, and $x_{i,t} = 0$ otherwise. Additionally, a binary variable $dr_t \in \{0, 1\}$ is introduced to represent system-level operational DR at time step t, where $dr_t = 1$ denotes that DR is applied, and $dr_t = 0$ corresponds to normal operation. The scheduling of O&M actions is illustrated in Fig. 9, where each component follows an independent degradation path but shares a common trigger for maintenance execution. This structure enables coordinated interventions that reduce logistical costs and downtime.

A second binary variable y_t is defined to represent the vessel mobilization status at time step t, where $y_t = 1$ if at least one component is scheduled for repair on day t, and $y_t = 0$ otherwise. This relationship is explicitly formulated through the following constraint:

$$y_t \geq x_{i,t} \tag{12}$$

$$y_t \leq \sum_{i=1}^{4} x_{i,t} \tag{13}$$

The constraints are designed to ensure that vessel mobilization occurs only when at least one repair is scheduled, thereby preventing unnecessary dispatches.

To promote opportunistic maintenance, an additional constraint is imposed such that each vessel dispatch must involve repairs on at least M components. This requirement is represented by the following condition:

$$\sum_{i=1}^{4} x_{i,t} \geq M \cdot y_t, \quad M \geq 2 \tag{14}$$

DR is considered as an alternative strategy applicable only when no repairs are scheduled, thereby ensuring a clear separation between repair activities and structural-level DR operations. This condition is: enforced by the following constraint:

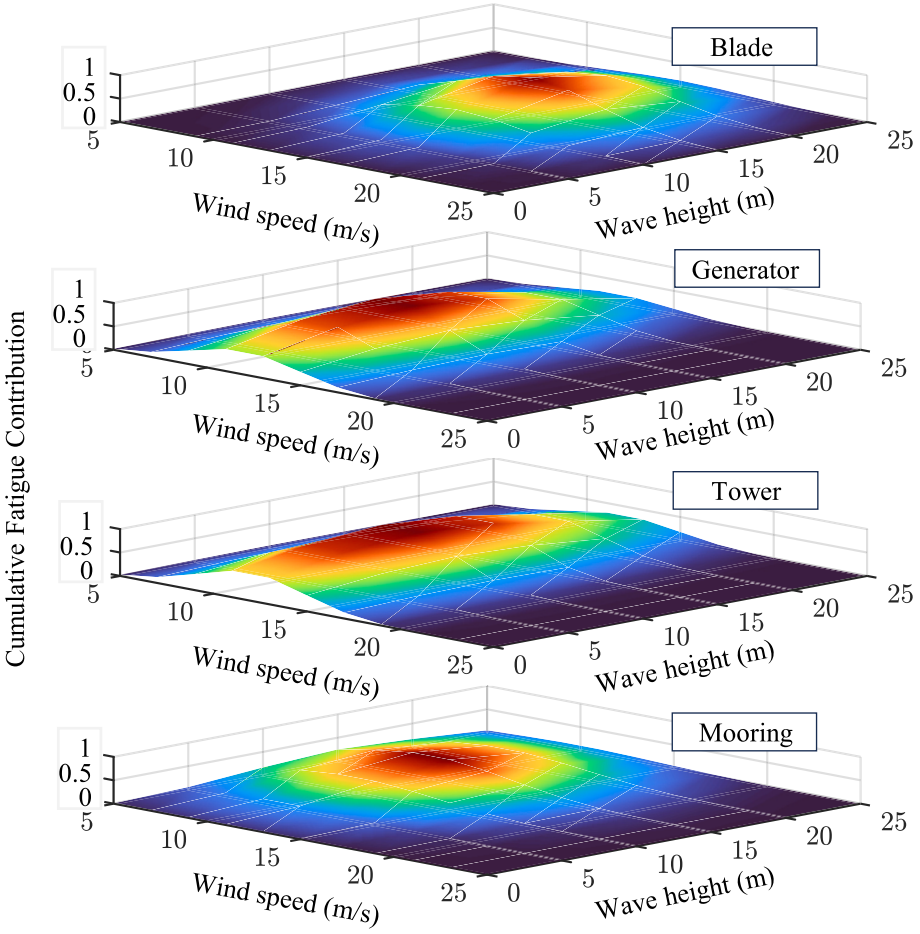

Fig. 16. CFC under different combinations of wind speed and significant wave height.

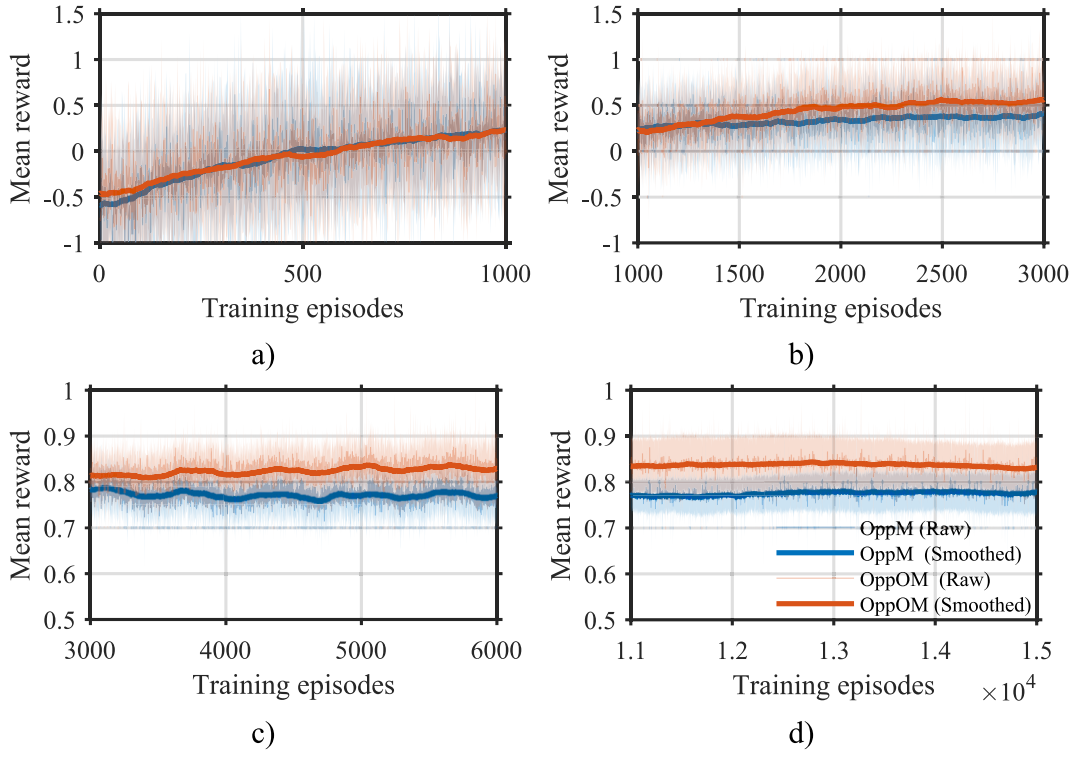

Fig. 17. Key training phase analysis of A3C in OppM and OppOM. a) initial exploration; b) rapid convergence; c) Fine tuning; d) Stable performance.

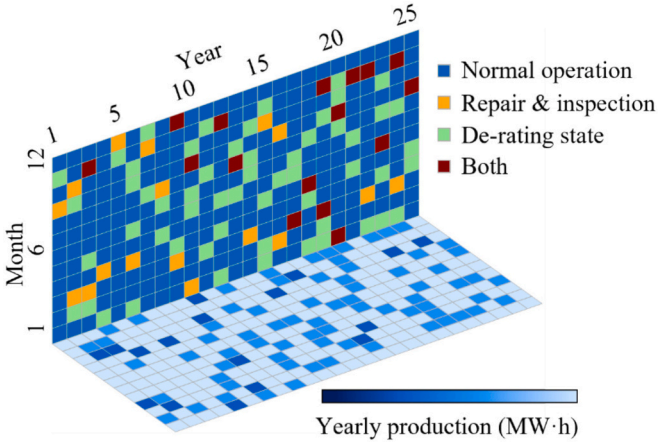

Fig. 18. Optimal OppOM schedule by the proposed DT framework with low-fidelity.

$$\sum_{i=1}^{4} x_{i,t} + dr_t \leq 1 \tag{15}$$

Repair actions are modeled explicitly as parallel activities, allowing multiple structural components to be serviced simultaneously during a single vessel dispatch. The total downtime on day t, denoted by τ_t, is determined by the maximum individual repair duration among all components scheduled for maintenance on that day.

$$\tau_t = \max_{i\in\{1,2,3,4\}} \{\tau_i \cdot x_{i,t}\} \tag{16}$$

By modeling repair actions as parallel processes, the total downtime and associated production losses are significantly reduced, thereby enhancing overall operational efficiency.

To ensure structural integrity and maintain safe operating conditions, the health level of each component, denoted by $HI_{i,t}$ is required to remain above a predefined threshold $HI_i^{\min}$ [117]. This condition is: enforced through the following constraint:

$$HI_{i,t} \geq HI_i^{\min} \tag{17}$$

To ensure holistic structural health, the minimum health level among all components must exceed a system-level threshold HI_{sys}^{min} at all times [118,119].

$$\prod_{i=1}^{4} HI_{i,t} \geq HI_{sys}^{\min} \tag{18}$$

4. Multi-objective optimization in FOWT O&M using deep reinforcement learning

4.1. Multi-attribute function on FOWT

Cevasco et al. [41] systematically investigated the relationship between structural reliability, plant availability, and maintenance actions in wind turbines. Their findings highlight that maintenance operations, while essential for long-term integrity, may induce significant downtime, thus impacting energy production and increasing lifecycle costs. This challenge becomes even more pronounced in offshore wind turbines, particularly in FOWTs, which exhibit deeply coupled system behavior [120]. Optimization in such systems must account for economic [121], structural [122], and stochastic interdependencies across subsystems [123,124], as well as the complex interactions among structural engineering, control strategies, hydrodynamics, and economic considerations. Consequently, decisions that optimize one metric (e.g., reducing carbon footprint) may unintentionally compromise others (e.g., increase lifecycle cost or reduce availability), rendering isolated evaluations insufficient [125]. A comprehensive, system-level maintenance framework is therefore required. As shown in Fig. 10, such a multi-attribute framework enables the quantification and governance of trade-offs across dimensions, supporting coherent decision-making in complex, multidisciplinary systems. This section introduces a comprehensive mathematical framework for the OppOM of FOWTs, aiming to optimize maintenance strategies that are both cost-efficient and structurally robust. The formulation coherently integrates key factors including maintenance timing, vessel deployment, operational disruptions, structural degradation, energy losses, and

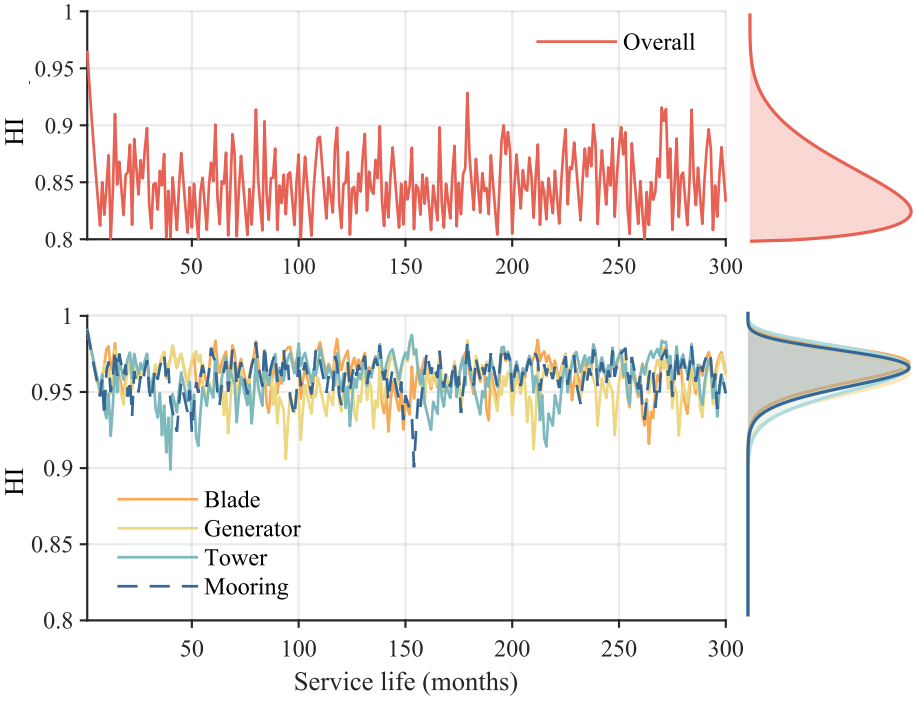

Fig. 19. HI development under the OppOM strategy of FOWT.

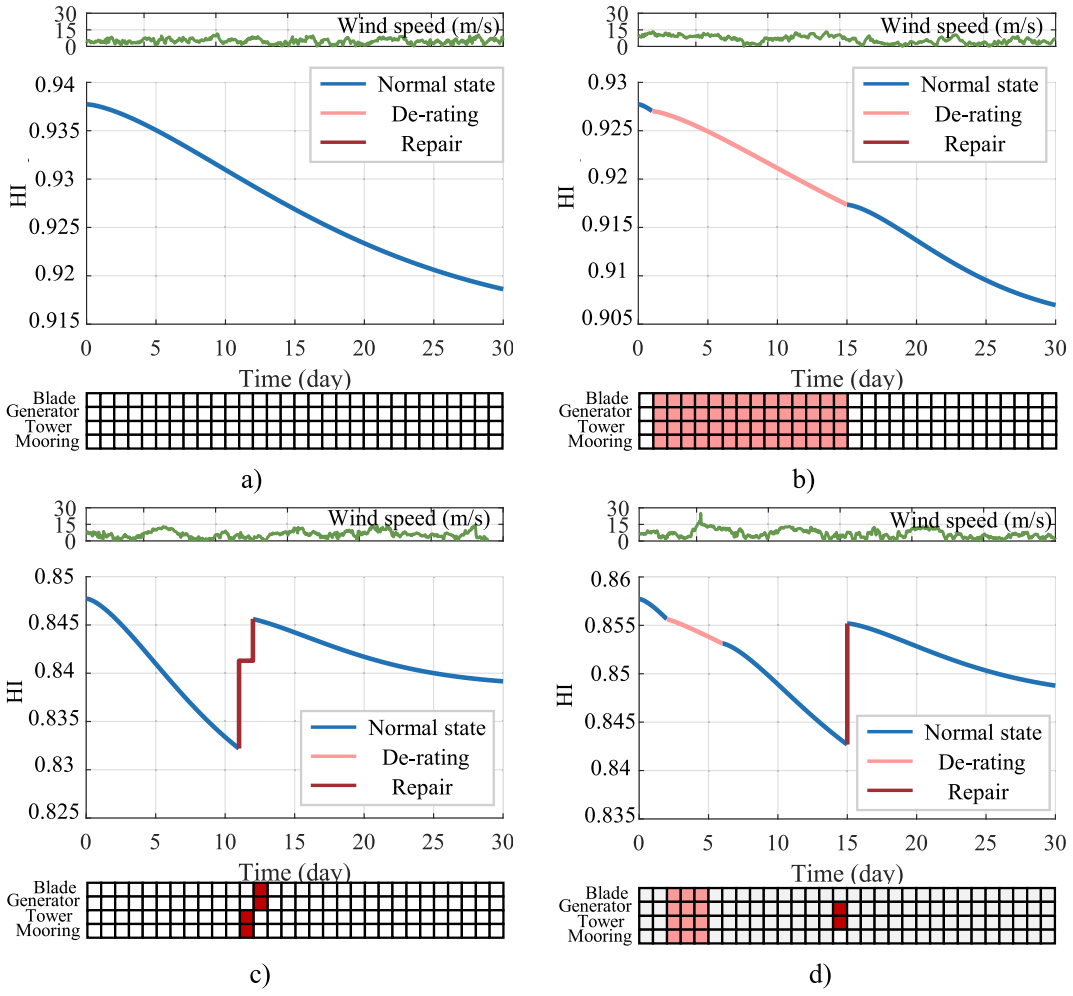

Fig. 20. Detailed performance development of four selected typical actions. a) Non-action; b) De-rating state; c) Repair action; d) Both action.

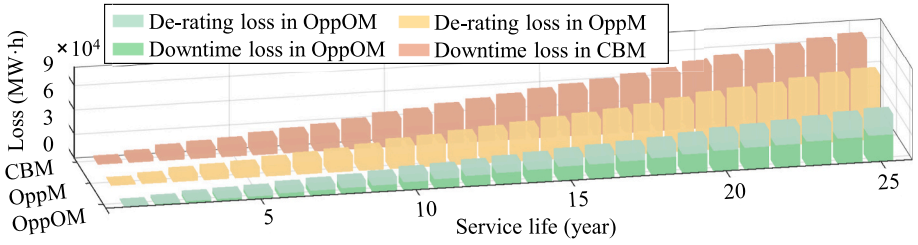

Fig. 21. Cumulative energy loss under different O&M maintenance strategies.

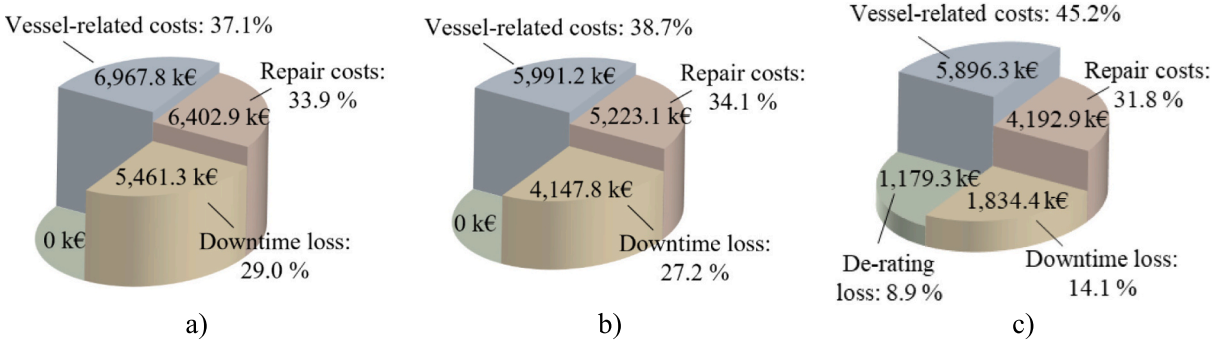

Fig. 22. Total cost and distribution under different O&M strategies. a) CBM; b) OppM; c) OppOM.

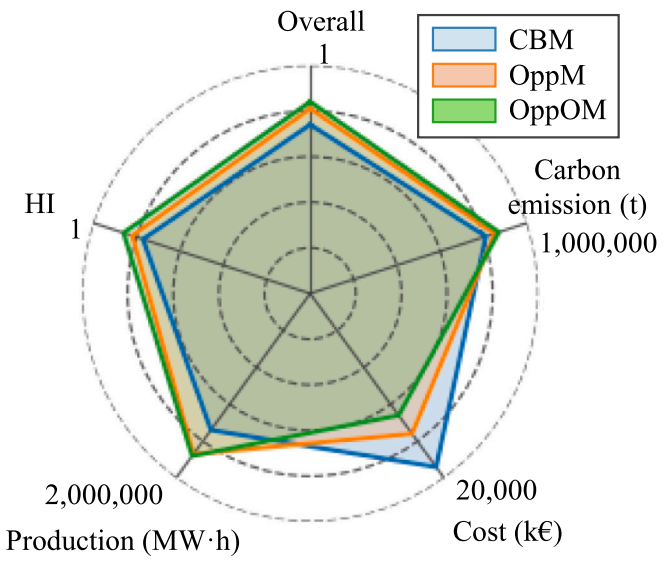

Fig. 23. Comprehensive performance of FOWT (CBM; OppM; OppOM).

Table 4
Summary of key modelling assumptions

Assumption	Eq./Sec	Rationale
Independence between natural degradation and crack growth.	Eq. (6)	A first-order approximation is adopted to obtain a tractable DBN and scalable inference. Marine corrosion–fatigue was not modelled separately; overall degradation was represented by a generalised Weibull distribution [105–107].
Stationary POD parameters	Eqs. (7)–(8)	A time-invariant logistic POD curve is assumed [108,109].
Parallel repairs; downtime = maximum single duration	Eqs. (12)–(16)	When a service vessel is mobilised, multiple tasks may be executed in parallel; outage for a cluster is approximated by the longest single task [110,111].
Constant and emissions factors	Eqs. (28)–(31)	Lifecycle-average valuation and grid-average emissions factors are used [112,113].
Representative meteorological years; stationary climate statistics	Site data	Representative wind–wave years reproduce long-term site statistics over the 25-year horizon [114,115].
Repair resets to health; de-rating modifies transitions	Sec. 2.2	Repairs are modelled as probabilistic restorations of component health [116], and de-rating modifies transition probabilities.

environmental impact.

4.1.1. Health state

The health state assessment of FOWTs is essential for maintaining operational safety and long-term reliability. This section proposes a structural health-based model that integrates external environmental loads, internal control strategies, and maintenance actions. This model quantifies the structural health state using a time-dependent index [126]. The structural health index $HI = 1 - PoF$ is directly computed at each time step using the formulation introduced in Section 2. This index captures the combined effects of degradation, loading conditions, and O&M actions, as determined by the corresponding analytical expression.

$$HI(t) = HI_0 - \gamma_1 t - \gamma_2 S(t) + \gamma_3 M(t) \tag{19}$$

where HI_0 is initial reliability; γ_1 denotes the natural degradation rate coefficient; γ_2 captures the effect of cumulative environmental loads; γ_3 measures the beneficial impact of maintenance; $S(t)$ is the cumulative environmental load up to day t; and $M(t)$ is the cumulative maintenance effect by day t.

The system-level HI follows a series composition

$$\mathrm{HI}_{\mathrm{sys}} = \prod_{i=1}^{n} \mathrm{HI}_i \tag{20}$$

In practice, a component-level safety constraint PoF $\leq$ 10%(i.e., HI $\geq$ 0.90) is adopted as an internal risk-based trigger [117], consistent with risk-based inspection and repair practice.

Maintenance actions are modeled as:

$$M(t) = \sum_{i=1}^{n} \delta_i \cdot z_{i,t} \tag{21}$$

where δ_i indicates the effectiveness of repairing component i; $z_{i,t}$ denotes whether component i is repaired on day t.

4.1.2. Power production

Power production is a key indicator of FOWT performance, directly linked to economic output and system efficiency. It is influenced by wind conditions, maintenance-induced downtime, and operational strategies such as DR.

The total energy produced on day t is:

$$E(t) = \int_0^{24} P(v(t,\tau))\cdot[1 - I_d(t,\tau)]\cdot\eta(t)\, d \tag{22}$$

where $I_d(t,\tau)$ is a binary indicator set to 1 if the turbine is shut down at time τ due to repairs or DR; $\eta(t)$ represents the system efficiency on day t, which is influenced by the health state; τ is the total downtime used to determine values of $I_d(t,\tau)$.

When structural DR is applied (i.e., $dr_t = 1$), the rated power is reduced:

$$P_{\mathrm{dr}}(t) = P_{\mathrm{rated}}\cdot(1 - \lambda(t)) \tag{23}$$

where $\lambda(t)$ is the DR coefficient (0–1).

The corresponding energy loss from DR is:

$$E_{\mathrm{dr}}(t) = E_{\mathrm{nom}}(t) - E_{\mathrm{dr}}(t) \tag{24}$$

4.1.3. Economic cost

This section develops a comprehensive economic framework that quantifies the financial implications of maintenance decisions, vessel logistics, production losses, and operational strategies such as power DR.

The total cost over a planning horizon T is defined as the sum of four major components [127,128]: vessel mobilization cost, repair cost of individual components, downtime-induced production loss, and energy loss due to DR:

$$C_{\mathrm{total}} = \sum_{t=1}^{T} \left[C_{\mathrm{dp}}(t) + \sum_{i=1}^{n} C_i(t)\cdot z_{i,t} + C_{\mathrm{dt}}(t) + C_{\mathrm{dr}}(t) \right] \tag{25}$$

where C_{total} is the cumulative economic cost over the time horizon T.

For each component, repair activities incur a cost $C_i(t)$ when executed at time t. The binary decision variable $z_{i,t} \in \{0,1\}$ indicates whether a repair is performed:

Thus, the total repair cost at time t is the sum of component-wise costs [129,130].

$$\sum_{i=1}^{n} C_i(t)\cdot z_{i,t} \tag{26}$$

Maintenance operations in offshore environments often require the dispatch of specialized vessels [34]. A binary variable $y_t \in \{0,1\}$ is introduced to indicate whether any component is repaired on day t. The vessel mobilization cost is modeled as:

$$C_{\mathrm{dp}}(t) = C_{\mathrm{ves}}\cdot y_t \tag{27}$$

where C_{ves} is the fixed mobilization cost for deploying a maintenance vessel.

While repairs are conducted, turbines are temporarily taken offline, leading to lost power generation and associated revenue loss. The downtime duration on day t is denoted by τ_t, and the corresponding cost is given by:

$$C_{\mathrm{dt}}(t) = c_{\mathrm{dt}} \cdot \tau_t \tag{28}$$

where c_{dt} is the unit downtime cost, reflecting the opportunity cost of unavailable energy. This cost includes both direct energy sales loss and potential penalties from unfulfilled energy contracts [131].

DR strategies, while beneficial in extending component life and reducing failure risk, result in a deliberate reduction of power output. On any day t, if DR is applied, energy production is curtailed. The resulting energy loss is denoted $E_{\mathrm{dr}}(t)$, and the associated cost is calculated as:

$$C_{\mathrm{dr}}(t) = c_{\mathrm{e}} \cdot E_{\mathrm{dr}}(t) \tag{29}$$

where c_{e} represents the unit price of electricity. This cost term captures the economic trade-off of applying DR, especially under high market prices or grid obligations.

4.1.4. Carbon emission

Carbon emissions are a key metric in environmental performance evaluation of FOWTs. This section considers both emission reductions from renewable energy production and emissions resulting from maintenance operations [132–134].

Carbon emission reduction is computed as:

$$CO_2^{\mathrm{red}}(t) = e_{\mathrm{trad}} \cdot E(t) \tag{30}$$

where e_{trad} is the emissions factor for displaced fossil energy.

Maintenance-related emissions are:

$$CO_2^{\mathrm{rep}}(t) = y_t \cdot e_{\mathrm{ves}} + \sum_{i=1}^{n} z_{i,t} \cdot e_{\mathrm{rep},i} \tag{31}$$

where e_{ves} indicates emissions from a single vessel deployment; $e_{\mathrm{rep},i}$ denotes the emissions from repairing component i.

The net carbon impact is:

$$CO_2^{net}(t) = CO_2^{red}(t) - CO_2^{\mathrm{rep}} \tag{31}$$

4.1.5. Multi-attribute function

As aforementioned, health state, energy production, economic performance, and carbon emissions are interrelated throughout the full lifecycle O&M of FOWTs. The coupling effects often lead to interdependent or conflicting relationships among factors. To manage such trade-offs, this study employs a multi-attribute utility (MAU) function [135], a method widely used in decision theory to incorporate risk preferences across multiple indicators. Each indicator is first normalized based on the decision-maker's risk attitude and then aggregated using a weighted utility function [136], typically expressed in exponential form (see Equation 33).

$$\mathrm{U_i(x_i)} = \mathrm{A} - \mathrm{B} \bullet \mathrm{e}^{-\frac{x_i}{RT}} \tag{33}$$

where U_i denotes the utility of indicator i; A and B are scaling constants determined by the indicator's value range; and RT represents risk tolerance, capturing the decision-maker attitude toward data uncertainty and failure risk. All four objectives were weighted equally, assigning a value of $1/N$ to each of them [137]. A detailed sensitivity analysis under alternative weight configurations is reported in Appendix C.

To enhance the economic interpretability of the proposed optimization framework the Levelized Cost of Energy (LCOE)is introduced to evaluate the cost-effectiveness of different O&M strategies [10,138]. In general, the total LCOE includes both capital expenditure and operational expenditure, as well as financial parameters such as depreciation, residual value, and financing cost. However, since the focus of this study lies in optimizing operational and maintenance decisions rather than investment planning, only the O&M-related portion of the LCOE is considered here. This O&M-specific LCOE (denoted as $\mathrm{LCOE_{O\&M}}$) provides a consistent measure for comparing maintenance policies by normalizing the lifecycle O&M cost with the corresponding total energy production:

$$LCOE_{O\&M} = \frac{C_{\mathrm{total}}}{E_{\mathrm{life}}} \tag{34}$$

where $C_{\mathrm{total}}$and E_{life}denote the total O&M cost and total energy generated over the turbine lifetime, calculated from Equations 22 and 25, respectively. The numerical results and comparison among strategies are presented in Section 5.4.

4.2. Deep reinforcement learning solution for OppOM

Traditional RL applications have predominantly focused on domains where features can be manually engineered or represented within low-dimensional state spaces. However, in the context of complex multi-component structural systems, the decision space expands exponentially with the number of components and control variables, posing a significant scalability challenge [139]. In this study, the FOWT system is decomposed into four distinct structural components, each requiring independent maintenance decision-making. Additionally, a global DR control variable influences the degradation trajectories of all components simultaneously. This combination of localized and system-wide decision factors leads to a high-dimensional, tightly coupled decision space. Consequently, conventional RL approaches are insufficient for directly handling such complexity, necessitating more advanced methods capable of managing large-scale, multi-agent decision environments [140]. To address this challenge, an asynchronous advantage actor-critic (A3C) strategy is employed to solve the high-dimensional DBN-POMDP formulation proposed in this study.

The A3C algorithm, proposed by DeepMind [141], builds upon the classical Actor-Critic (AC) framework by introducing asynchronous parallel training across multiple agents. As illustrated in Fig. 11, the AC method comprises two primary components: the actor and the critic [142]. The actor, implemented as a policy network, selects actions according to the current policy, while the critic, implemented as a value network, evaluates these actions by estimating the value function. The actor updates the policy to maximize the expected cumulative reward, whereas the critic refines the value estimates to better predict future returns, thereby providing a baseline that helps reduce the variance of policy gradient updates [143].

Initially, the actor's policy $\pi(a|s;\theta)$ and the critic's value function $V(s;\omega)$ are parameterized by randomly initialized weights θ and ω, respectively. At each time step t, the actor selects an action a_t according to the current policy:

$$a_t \sim \pi(a|s_t;\theta_t) \tag{35}$$

Upon executing the action, the environment transitions to a new state s_{t+1} and returns a reward r_t. The critic then evaluates the new state by estimating its value $V(s_{t+1};\omega_t)$, and the temporal-difference (TD) error is computed as:

$$\delta_t = r_t + \gamma V(s_{t+1};\omega_t) - V(s_t;\omega_t) \tag{36}$$

The critic updates its parameters using the TD error via the following update rule:

$$\omega_{t+1} = \omega_t + \alpha_c \delta_t \nabla_\omega V(s_t;\omega_t) \tag{37}$$

where α_c denotes the learning rate of the critic. Simultaneously, the actor updates its policy parameters to reinforce advantageous actions:

$$\theta_{t+1} = \theta_t + \alpha_a \delta_t \nabla_\theta \log\pi(a_t|s_t;\theta_t) \tag{38}$$

where α_a is the learning rate for the actor.

At each step, the actor selects an action based on the current policy, resulting in a transition of the environment to a new state and the generation of a reward signal along with updated observations. The immediate reward r reflects a trade-off between the cost of the action and the associated benefits [144]. This reward is computed according to the multi-attribute utility function introduced in Section 4.1. In the formulation, the production-related component of the reward is an instantaneous function of the prevailing wind conditions, which exhibit strong serial correlation. Consequently, maintenance decisions depend not only on immediate cost considerations but also on anticipating future production opportunities under evolving environmental and degradation states. The critic uses this feedback to refine its estimate of the value function, while the actor updates the policy accordingly to improve future decision-making.

Building on the AC framework, the A3C algorithm enhances training efficiency and scalability by enabling multiple agent-environment interactions to occur in parallel, each handled by an independent worker thread [145]. As illustrated in Fig. 12, each worker thread maintains a local copy of the global policy $\pi(a|s;\theta)$ and value function $V(s;\omega)$. During training, each worker thread interacts with its own instance of the environment, collecting trajectories of state-action-reward sequences (s_t, a_t, r_t) [146].

For each local interaction, the worker computes gradients with respect to its current policy and value networks . Specifically, the policy gradient for a single worker is estimated using the advantage function:

$$A(s_t, a_t) = r_t + \gamma V(s_{t+1}; \omega_t) - V(s_t; \omega_t) \tag{39}$$

The corresponding gradient for the policy network is given by:

$$\nabla_t J(\theta) = \nabla_\theta \log \pi(a_t s_t; \theta) \cdot A(s_t, a_t) \tag{40}$$

Similarly, the value network parameters are updated using the temporal-difference error:

$$\nabla_t L(\theta_v) = \frac{\partial}{\partial \theta_v} \left[\left(r_t + \gamma V(s_{t+1}; \omega_t) - V(s_t; \omega_t) \right)^2 \right] \tag{41}$$

These local gradients, denoted in the diagram as $\nabla_0 J(\theta)$,$\nabla_1 L(\theta)$, …,$\nabla_{nL}(\theta)$, are asynchronously sent to a global model. The global policy and value parameters are then updated without waiting for synchronization across all workers:

$$\theta \leftarrow \theta + \alpha_a \sum_{i=1}^{n} \nabla_i J(\theta) \tag{42}$$

$$\theta_v \leftarrow \theta_v - \alpha_c \sum_{i=1}^{n} \nabla_i L(\theta_v) \tag{43}$$

By decoupling data collection from global updates and leveraging diverse exploration paths across workers, A3C avoids the inefficiencies of experience replay and mitigates the risk of policy collapse. The asynchronous updates from multiple agents collectively contribute to more stable and generalized policy learning, making A3C especially well-suited for high-dimensional decision-making problems such as the DBN-POMDP formulation introduced in this study.

5. Results and discussion

5.1. Investigated FOWT and environmental condition

A 15 MW wind turbine mounted on a US-semi substructure is selected as the reference system for analysis [147,148]. The turbine is modeled using OpenFAST [149], and the distributions of key dynamic responses under varying wind speeds are extracted. The response characteristics exhibit clear structural specificity across different components. For the blade (Fig. 13a), the presence of the yaw control system maintains an upwind-facing configuration, resulting in a strong positive correlation between wind speed and extreme response magnitude. In contrast, the tower response (Fig. 13b) displays a non-monotonic pattern: increasing with wind speed up to a peak near the rated wind velocity (10.59m/s [148]), followed by a gradual decline, a trend consistent with findings reported in [150]. The generator response (Fig. 13c) follows a broadly similar trend to that of the tower, yet as a critical interface between the blade and tower systems, it also exhibits blade-like features. Specifically, the response distribution is more concentrated at low wind speeds but becomes increasingly dispersed as wind intensifies. Finally, the mooring line (Fig. 13d), being submerged, is influenced by both the upper platform's motion and wave-induced loading [151]. This dual dependency leads to pronounced variability in its dynamic response, manifesting as high statistical dispersion.

The condition site selected is Station CAPE ELIZABETH, located approximately 83.34 kilometers northwest of Aberdeen, Washington, with a water depth of about 131 meters [152]. As shown in Fig. 14, wind speed and significant wave height records from 1988 to 2023 in the selected region indicate that the majority of conditions fall below 15 m/s, corresponding to a medium-to-low wind regime. In conjunction with Fig. 13, it can be observed that most extreme structural responses occur within the rated wind speed range. This suggests that a proper DR strategy can effectively mitigate high-amplitude loads during the turbine's service life. Moreover, wind speed and wave height exhibit a clear monotonic relationship in this region, where high wave conditions generally coincide with high wind speeds.

5.2. Long-term degradation of FOWTs

Fig. 15 presents the natural degradation trajectories of key components over the life-cycle of the turbine. The reliability index β is employed to quantify the inherent degradation state of the structure, with β=2 selected as the failure threshold to indicate structural failure under natural operating conditions [98]. For clarity, β in this section is used here only to compare degradation patterns under natural operating conditions; OppOM decisions rely exclusively on *HI* and the component-level safety constraint.

The deterioration patterns exhibit substantial heterogeneity across components. Specifically, the blades and generator undergo relatively rapid degradation during the early operational phase, with cumulative damage reaching critical thresholds at approximately 14 to 15 years. In contrast, the tower and mooring system experience more gradual degradation initially, followed by a sharp increase in failure probability during later stages. The tower approaches its critical limit at around 19.2 years, while the mooring system enters an accelerated degradation phase after approximately 16.3 years. This component-level disparity in aging behavior provides a theoretical foundation for optimizing maintenance intervals. By tailoring maintenance schedules to the specific degradation dynamics of each subsystem, it is possible to both delay the onset of critical damage in vulnerable components and reduce overall actions.

To further examine the influence of varying wind speeds and wave conditions on structural fatigue, Fig. 16 illustrates the Cumulative Fatigue Contribution (CFC) under different combinations of wind speed and significant wave height [153]. For the FOWT blades, the CFC generally increases with rising wind speed and wave height, a trend primarily driven by the yaw control system, which consistently orients the blades into the wind. As wind speed increases, aerodynamic loading intensifies, leading to higher fatigue contribution. However, the CFC peaks at around 15 m/s, after which it declines sharply and becomes negligible beyond 23 m/s. This is largely due to the local wind climate: high wind speed events are infrequent and therefore contribute little to long-term fatigue accumulation. In contrast, both the generator and tower exhibit peak CFC values near the rated wind speed, reflecting the combined influence of pitch control strategies and wind speed distribution. A subtle difference is observed in the tower response: at elevated wind speeds, high wave heights significantly amplify fatigue, resulting in a skewed CFC distribution toward the upper wind-wave regime. For the mooring system, although rated wind speed has some effect, the CFC

is primarily driven by wave height distribution. Consequently, the CFC curve appears smoother with lower peaks, reflecting a more gradual fatigue accumulation process.

5.3. Opportunistic O&M scheduling

To assess the performance enhancement offered by the proposed operation and maintenance co-optimization strategy (OppOM) over the conventional opportunistic maintenance-only approach (OppM), a comparative analysis was conducted. All DR trigger variables introduced in Section 3.2 were fixed at zero, thereby reducing the OppOM framework to a pure OppM formulation. The CBM strategy was treated as an external benchmark and excluded from the optimization process. The DBN-POMDP is solved with an A3C agent using Adam optimizers for both actor and critic. Table 5 lists all training hyperparameters, consistent with typical A3C implementations reported in previous studies [154,155]. For the discount factor, under the *HI* constraints imposed in this formulation, the optimal action interval is naturally restricted to approximately 200–300 days, which is fully contained within the effective decision horizon of $\gamma = 0.99$. A full sensitivity analysis over $\gamma \in \{0.98, 0.99, 0.995, 0.999\}$ is reported in Appendix B. All experiments were conducted on a workstation equipped with an Intel® Core™ i7-13700 CPU (16 cores, 24 threads, base frequency 2.1 GHz, turbo up to 4.9 GHz), 32 GB of system memory, and an NVIDIA® GeForce RTX 4070 Ti GPU.

The proposed DBN–POMDP–A3C framework was trained under a specific condition site, representing a particular operational environment of FOWT management. All training processes were conducted offline using simulated deterioration transitions to obtain an optimal O&M policy. Model initialization required 14 min 48 s, and the asynchronous training of 15000 episodes converged within 17 h 13 min 26 s. The evaluation and visualization of training performance consumed 24 min 32 s, with a peak memory footprint of 9.8 GB RAM and 4.7 GB GPU memory. After training, the framework performs online inference under selected condition site, where the trained actor network generates O&M decisions through a single forward pass without parameter updates. Each decision is produced within 28.4 *ms* on GPU and 52.6 *ms* on CPU, indicating the potential for real-time decision support once deployed. Although the present work focused on offline training and planning for specific site rather than implementing a real-time operational system, similar frameworks have been applied in the energy domain with real-time or near-real-time performance. For instance, Liu et al. applied a DRL-based controller for real-time economic energy management in powertrain, achieving sub-second decision latency under uncertainty [156]; Alabi et al. proposed an automated DRL agent for real-time multi-energy scheduling that achieved responsive control in distributed energy systems [157].

Table 5
A3C Training configuration for OppOM and OppM

Item	Value
Optimizer (both actor & critic)	Adam
Actor learning rate α_a	1e-5
Critic learning rate α_c	1e-4
Discount factor γ	0.99
Workers (threads)	4
Update horizon t_{max}	20 steps
Replay buffer	None
Entropy bonus	0
Value loss weight	0.5
Grad clipping	Not applied
Batch per update	Trajectory of $\leq$10 steps/worker
Episodes / worker	15000
Network (Actor)	[1024, 512, 512] ReLU → logits
Network (Critic)	[1024, 512, 512] ReLU → 1
Initialization	Framework defaults (Glorot) [154]
Adam defaults	$(\beta_1 = 0.9, \beta_2 = 0.999, \epsilon = 1e-7)$

Fig. 17 illustrates the convergence behavior of the two strategies under the A3C learning framework. The mean reward, both raw and smoothed, was used as the primary performance metric. In the initial exploration phase (episodes 0–500), both strategies began with average rewards near –0.5, accompanied by considerable variance. Due to a lower-dimensional action space, the OppM strategy exhibited relatively narrower fluctuations. During the rapid ascent phase (episodes 1,000–3,000), improved environmental feedback was progressively captured. The OppM strategy demonstrated a steeper learning gradient owing to its simpler decision structure. In contrast, the OppOM model, characterized by a higher-dimensional action space, exhibited more gradual reward improvement, yet surpassed OppM performance around episode 3,000. In the subsequent stabilization phase (episodes 3,000–6,000), the learning curves of both models leveled off, with OppM oscillating around 0.75 and OppOM stabilizing near 0.80. A marked reduction in variance was observed for both, indicating improved policy robustness. By the final steady-state phase (episodes 11,000–15,000), OppM converged at a mean reward of approximately 0.77, whereas OppOM reached 0.84.

Although the OppOM strategy required more iterations to converge due to increased complexity, a superior long-term reward was ultimately attained. These results validate the effectiveness of integrating operational flexibility with maintenance planning, yielding more optimal system-level outcomes than maintenance-only strategies. Fig. 18 further illustrates the distribution of various O&M states under the OppOM strategy over a 25-year service life. It is observed that the structure remains in a stable operational state for the majority of its lifetime. During the first five years, only minimal repair actions are required to maintain functionality, with a single occurrence of DR observed. As service time progresses, the frequency of DR events increases noticeably. However, the frequency of repair actions remains relatively unchanged, suggesting that the implemented strategy effectively slows the overall degradation rate of structural components. In the final five years of operation, a more pronounced rise is observed in both DR and repair frequencies, indicating the onset of accelerated aging in multiple subsystems. Importantly, the power output of the turbine remains consistently stable throughout the entire service period. Even during months when DR or repair actions are triggered, no significant drop in generation is detected. This indicates that the OppOM strategy ensures robust operational continuity, maintaining high energy production despite maintenance events.

HI development under the OppOM strategy is illustrated in Fig. 19, showing both component-level and system-level performance across the full 25-year service life (12 × 25 months). The overall structural HI remains consistently high, with values exceeding 0.8 throughout the entire period, and the trajectory closely approximates a positively skewed normal distribution, reflecting gradual and controlled degradation. At the component level, all major subsystems maintain HI indices above 0.9, indicating strong structural resilience under the OppOM framework. These results confirm that the proposed strategy substantially improves life-cycle safety performance of FOWTs. Furthermore, analysis of specific time points reveals that whenever a maintenance or DR action is triggered, multiple components are typically involved. This demonstrates that the proposed algorithm is capable of effectively identifying and clustering maintenance opportunities, ensuring that each offshore intervention addresses multiple repair tasks simultaneously. Such task aggregation improves resource utilization and reduces the number of offshore visits required over the operational life.

Further insights into the behavior of the proposed framework are provided in Fig. 20, which depicts the evolution of the reliability index during representative months under different operational conditions. In Fig. 20a, a relatively calm month with low wind speeds is shown. The degradation progresses slowly, and the reliability index closely follows a Weibull-like distribution, reflecting the baseline aging trend in low-stress environments. Fig. 20b captures a month during which DR occurred between days 2 and 15. A notably slower degradation trend is

observed, despite sustained wind speeds approaching 15 m/s throughout the DR period. This suggests that the optimization algorithm proactively activates DR actions to mitigate accelerated structural fatigue during high-wind intervals. Fig. 20c illustrates a month characterized by repair-only events. A two-day offshore maintenance task was carried out, during which all four major components underwent restoration. The corresponding wind speeds remained in the low-to-moderate range, ensuring both the safety of on-site operations and the minimization of downtime-related energy loss. Fig. 20d presents a scenario in which both DR and repair actions were triggered. Here, DR was deployed prior to the activation of maintenance thresholds, effectively delaying structural degradation. Notably, the A3C-based optimization framework succeeded in scheduling DR actions during high-wind periods while deferring maintenance to lower-wind intervals, optimizing both structural longevity and operational availability. The observations collectively underscore the capability of the proposed A3C-based control policy to function as a dynamic and integrated operation-maintenance coordination framework. By simultaneously accounting for wind resource conditions and structural health states, the framework enables the deployment of adaptive O&M strategies that are both responsive and resource-efficient.

5.4. Performance evaluation of O&M strategies: energy, cost, and multi-criteria analysis

As discussed in Section 4.1, both economic losses and carbon mitigation potential in FOWTs are directly linked to power generation capacity. Consequently, the trade-off between DR-induced production loss and downtime-related loss plays a critical role in determining overall system performance. Fig. 21 presents the cumulative production loss under different strategies. For the OppOM framework, losses attributed to DR and maintenance downtime are found to be comparable over the full service life. Notably, the total production loss over 25 years under OppOM is 64,121.28 MWh, representing a substantial reduction compared to 116,197.87 MWh under CBM and 88,251.06 MWh under OppM, equivalent to 44.82% and 27.34% improvements, respectively. The results indicate that the proposed OppOM strategy significantly enhances wind energy utilization efficiency by effectively minimizing cumulative generation loss. From a life-cycle perspective, strategically applying DR to mitigate structural degradation and to partially substitute conventional maintenance efforts offers a cost-effective and performance-driven solution.

Fig. 22 presents a breakdown in total life-cycle costs under different strategies, with all losses evaluated from an economic perspective. The analysis includes costs associated with offshore maintenance vessel deployment, direct repair expenses, and production losses caused by downtime and DR. The CBM strategy consistently incurs the highest cost, with total expenditures reaching €18,832k, primarily due to frequent offshore inspections required to sustain structural performance. In contrast, the OppM strategy reduces total costs to €15,352.1k by effectively managing maintenance triggers and limiting downtime. As a result, downtime-related production loss is curtailed to €4,147.8k. The OppOM strategy achieves the lowest life-cycle cost, amounting to €13,102.6k. By strategically integrating DR actions into the broader O&M framework, structural degradation is mitigated, leading to fewer required maintenance interventions. Although DR introduces moderate power losses, the combined economic impact from DR and downtime is limited to €3,013.7k, substantially lower than the corresponding losses under CBM and OppM. These findings highlight the cost-effectiveness of DR as an operational strategy. The intentional sacrifice of a limited amount of power generation can be compensated by a marked reduction in maintenance-related expenditures, resulting in improved overall economic efficiency. A comprehensive performance assessment across multiple dimensions is further illustrated in Fig. 23.

To quantify the economic performance of different O&M strategies, the *LCOE* was calculated using the simulated lifecycle total O&M costs and cumulative energy outputs. Table 6 summarizes the results:

Table 6
Comparison of LCOE and performance under different strategies.

Strategy	Total O&M Cost (k€)	Lifetime Energy (MWh)	*LCOE*
CBM	18,832	1,480,232	12.72
OppM	15,352	1,647,823	9.32
OppOM	13,103	1,661,122	7.89

The proposed OppOM strategy achieves the lowest $LCOE_{O\&M}$, corresponding to a 38% reduction relative to the baseline CBM approach. This improvement results from reduced unplanned downtime, more efficient vessel scheduling, and a slight increase in total power generation. It is acknowledged that a complete LCOE analysis should include capital investment, financing, and decommissioning costs. Nevertheless, within the O&M optimization context, the operational component represents the most directly influenced cost factor. The results therefore highlight that OppOM can effectively reduce the O&M cost per unit of electricity produced, contributing to improved lifecycle profitability and competitiveness of FOWTs.

Furthermore, Fig. 23 summarizes the distribution of key performance indicators over the 25-year service life for all three O&M strategies. Across all metrics, the proposed OppOM strategy consistently outperforms the baseline methods. The overall multi-criteria performance scores for OppOM, OppM, and CBM are 0.84, 0.81, and 0.74, respectively. In terms of structural health, the CBM approach—based on independent monitoring of each component and reactive maintenance upon threshold violation—exhibits limited degradation coordination and redundancy management. As a result, the average lifetime *HI* under CBM remains at 0.82. By contrast, both OppM and OppOM leverage opportunistic repair opportunities to perform preventive maintenance on components nearing, but not yet exceeding, damage thresholds. This proactive behavior improves overall system health, resulting in *HI* of 0.84 for OppM and 0.87 for OppOM. From a generation and environmental perspective, CBM performs the least efficiently due to frequent offshore deployment, prolonged downtime, and suboptimal operational scheduling. Over 25 years, its total energy production amounts to 1,480,231.7 MWh, corresponding to a net carbon reduction of 767,358.4 t CO_2. Both OppM and OppOM demonstrate clear advantages in cost, availability, and carbon impact, attributed to fewer offshore interventions and improved task coordination. Although their mechanisms differ slightly, OppOM integrates DR as a degradation-mitigation tool, enabling longer component life at the cost of marginally reduced power output. However, over the full lifecycle, this trade-off results in net performance gains. Specifically, the OppOM strategy achieves the highest energy yield at 1,661,121.5 MWh, along with a carbon offset of 853,541.1 t CO_2, surpassing the OppM strategy, which yields 1,647,823.3 MWh and 825,194.3 t CO_2 in net emission reductions.

6. Conclusions

A comprehensive life-cycle O&M framework was developed for FOWTs, integrating long-term structural degradation modeling, real-time probabilistic inference, and deep reinforcement learning-based optimization. The proposed OppOM strategy, which synergizes de-rating control with opportunistic repair scheduling, provides a unified approach to manage economic cost, structural health state, and environmental performance. Evaluation across multiple dimensions confirms that life-cycle-aware coordination enables superior long-term outcomes compared to conventional maintenance paradigms. The major findings are as follows:

1) A dynamic Bayesian network (DBN) was used to capture the probabilistic evolution of structural degradation over time, allowing for robust forecasting and uncertainty-aware risk assessment throughout the lifespan.

2) A DBN-POMDP-based optimization model, solved using the A3C algorithm, enabled intelligent action planning under partial observability, accounting for both real-time health inference and cumulative long-term objectives.
3) Component-level degradation heterogeneity was revealed, with blades and generators degrading earlier and towers and mooring systems failing later. This supports life-cycle adaptive maintenance scheduling and resource prioritization.
4) De-rating was validated as a viable long-term control strategy, effectively mitigating degradation during high-load conditions. Its coordinated use with maintenance reduced cumulative downtime without compromising system availability.
5) Full life-cycle cost analysis showed that OppOM reduced total expenditures to €13,102.6k, a 30.4% reduction compared to CBM. Production losses due to downtime and de-rating were minimized through balanced, anticipatory interventions.
6) Life-cycle performance indicators, including cumulative power generation (1,661,121.5 MWh), carbon mitigation (853,541.1 t CO_2), and average *HI* (0.87, with 0.969, 0.957, 0.973, and 0.965 for blade, generator, tower, and mooring), confirm that OppOM achieves optimal trade-offs between operational continuity, structural safety, and sustainability goals.

This study establishes a comprehensive, life-cycle-aware O&M optimization framework for FOWTs that integrates structural health, operational control, and economic-environmental trade-offs. The proposed OppOM strategy demonstrates significant advantages in reducing long-term costs and improving system availability through the coordinated use of de-rating and maintenance. The results confirm that intelligent, adaptive decision-making under uncertainty can outperform conventional approaches across multiple performance dimensions. Future work will extend the present framework from an integrated O&M optimiser to a digital twin that co-evolves with the turbine throughout its lifetime. Progress toward this goal involves incorporating coupled deterioration physics, uncertainty in structural assessment, maintenance resource competition and the shifting economic and environmental landscape shaped by climate change.

CRediT authorship contribution statement

Jiaxin Zhang: Writing – original draft, Visualization, Investigation, Formal analysis, Data curation. **You Dong:** Writing – review & editing, Resources, Methodology, Funding acquisition, Conceptualization. **Dan M. Frangopol:** Writing – review & editing, Supervision. **Songye Zhu:** Writing – review & editing, Funding acquisition. **Hongxing Yang:** Writing – review & editing, Supervision.

Declaration of competing interest

The authors declare that they have no known competing financial interests or personal relationships that could have appeared to influence the work reported in this paper.

Acknowledgment

The authors would like to acknowledge the financial support from the Research Grants Council (Research Impact Fund (RIF) project, R1006-23 and R5006-23), HKSAR, China. These supports are greatly appreciated. Any opinions, findings, and conclusions expressed in this material are those of the investigators and do not necessarily reflect the views of the sponsors.

Appendix A. Influence of crack-growth model on the O&M optimisation results

A.1. Appendix A1: Corrosion–fatigue versus adopted crack growth model in marine environments

This Appendix introduces a corrosion–fatigue (C–F) model derived from our previous work [98]. The model captures the coupled deterioration mechanisms experienced by offshore wind turbine structures in marine environments. Rather than assuming a single fatigue-driven Paris regime, the C–F formulation treats crack evolution as a sequential process comprising three phases, as shown in Fig A1a): an early corrosion-controlled initiation stage, followed by a transition phase in which corrosion and fatigue compete for dominance, and ultimately a late-stage propagation phase governed primarily by cyclic loading. Denoting the crack depth by $a(t)$at exposure time t, this three-stage formulation provides a more realistic description of crack growth under the combined influence of corrosive attack and cyclic stresses. At the initial stage, the crack is small, and the driving force is governed primarily by corrosion damage. Surface dissolution and pitting reduce the local resistance, whereas the contribution of cyclic loading remains limited because the stress-intensity factor range is below the validity threshold. The uniform corrosion loss is expressed as $D_{\mathrm{cor}}(t) = r_{\mathrm{cor}}\, t^{\beta}$, and the pit depth is approximated by

$$a_{\mathrm{pit}}(t) = \omega_{\mathrm{pit}} D_{\mathrm{cor}}(t) \tag{A.1}$$

Fatigue effects are added to the corrosion contribution based on rainflow-counted stress ranges $(\Delta\sigma_i, n_i)$, leading to the Stage 1 formulation

$$\frac{\mathrm{d}a}{\mathrm{d}t} = \left(\frac{\mathrm{d}a}{\mathrm{d}t}\right)_{\mathrm{cor}} + \left(\frac{\mathrm{d}a}{\mathrm{d}t}\right)_{\mathrm{fat}} \tag{A.2}$$

As the crack grows to an effective initial flaw size (EIFS), the fatigue-related crack growth rate becomes applicable, and corrosion and fatigue mechanisms coexist. The contribution of corrosion gradually decreases with $t^{\beta-1}$, whereas the fatigue driving force increases. Therefore, Stage 2 is defined by the dominant mechanism at each instant:

$$\frac{\mathrm{d}a}{\mathrm{d}t} = max\left[\left(\frac{\mathrm{d}a}{\mathrm{d}t}\right)_{\mathrm{cor}}, \left(\frac{\mathrm{d}a}{\mathrm{d}t}\right)_{\mathrm{fat}}\right] \tag{A.3}$$

When fatigue fully supersedes corrosion, the crack enters Stage 3, and the propagation follows the Paris-type law, as shown in Equation 2-3. Corrosive effects are incorporated through amplification of the Paris coefficient rather than the exponent:

$$A_{\mathrm{fcg,CF}} = C_{\mathrm{EAF}} A_{\mathrm{fcg,air}}, C_{\mathrm{EAF}} = 1 + 2\frac{r_{\mathrm{cor}}}{r_{\mathrm{cor0}}} \tag{A.4}$$

where r_{cor0} is the baseline corrosion rate associated with the designated corrosivity category. Thus, corrosion accelerates the crack growth in Stage 3

by increasing the fatigue crack-growth coefficient. The temporal evolution of crack depth in the tower was evaluated under the same site conditions as those used in Section 5 to ensure consistency with the main analysis.

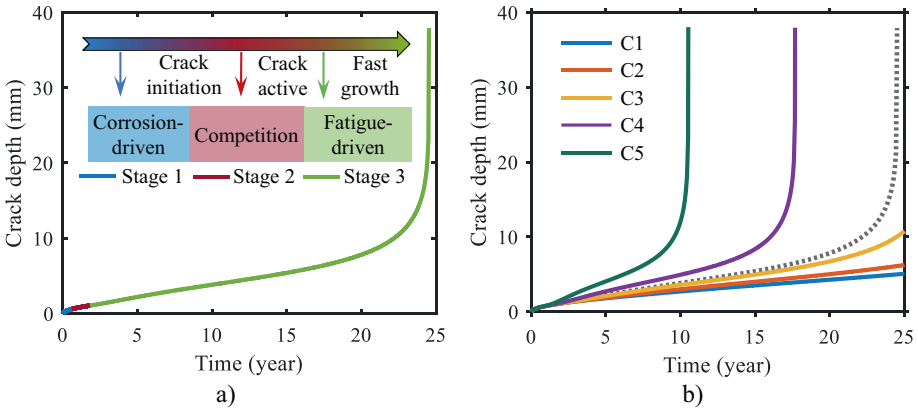

Fig. A1. Three-stage C–F crack evolution: a) progression under the site condition and b) variation across ISO corrosivity categories (C1–C5).

Fig. A1a) illustrates the temporal evolution of crack depth predicted by the proposed three-stage C–F model. Under the chosen site conditions, the corrosion-controlled initiation phase reaches the threshold crack size within roughly one year, after which the system transitions into the competition phase where the crack grows slowly. Once the propagation phase is entered, growth remains modest initially but accelerates sharply at later times as corrosion and cyclic loading act concurrently. Given the pronounced influence of the corrosive environment, Fig. A1b) compares the predicted crack evolution against the five corrosion categories defined in the ISO standard [158]. The grey dashed line corresponds to the site condition adopted in this study and lies between C3 and C4. Low-corrosivity environments (C1–C3) lead to negligible progression over a 25-year service life, whereas high-corrosivity environments (C4–C5) may result in rapid crack propagation to failure within the same timeframe. These comparisons demonstrate that the predictions of the C–F formulation are inherently coupled to the environmental conditions.

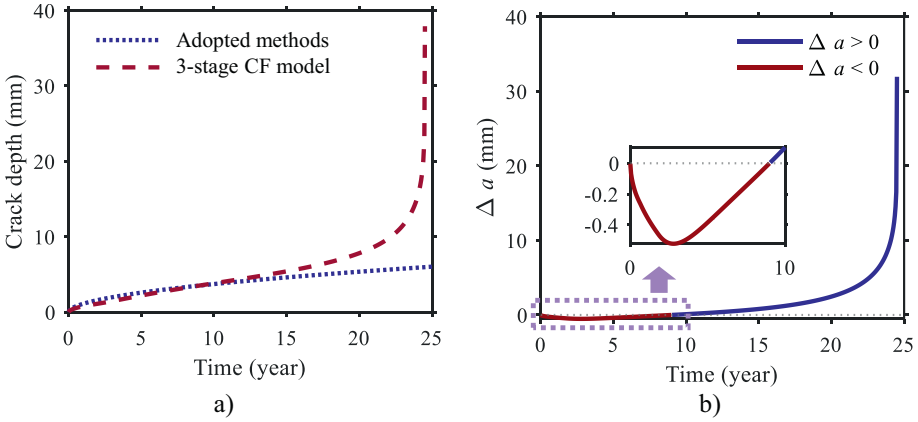

Fig. A2. Crack evolution under the 3-stage CF model versus the adopted formulation: a) crack-depth development and b) deviation Δa over time.

Fig. A2a) compares the crack evolution predicted by the proposed three-stage CF model with that obtained using the crack-growth formulation adopted in the main text. The two predictions are almost indistinguishable during the early period, whereas after approximately 10 years the CF model exhibits a markedly accelerated growth rate due to the increasing interaction between corrosion and fatigue, eventually leading to a rapid failure stage toward the end of service. Fig. A2b further highlights this difference through the deviation term $\Delta a = a_{CF} - a_{adopted}$, showing that the CF model even predicts a slightly slower crack-growth rate during the early phase, but later exceeds the adopted model substantially once natural degradation becomes dominant. It is worth noting that the primary focus of this study lies in the development of an O&M optimization framework, where timely interventions (repairs and/or de-rating) prevent the structure from entering the late-life accelerated propagation regime. Consequently, the crack-growth model adopted in the main text tends to provide a conservative basis for O&M decision-making, prompting actions before the sharply amplified CF phase.

Moreover, as shown in Equations A.1–A.4, the corrosion–fatigue formulation partitions degradation into three mechanistic stages, each dominated by a different governing law. The resulting three-stage crack model is a non-stationary degradation process with regime switching, discontinuous propagation rates and explicit max-operators, and requires multiple time-varying inputs [159]. These characteristics contrast sharply with the DBN–POMDP architecture used in the main text, which assumes stationary and factorable conditional transition probabilities [160], making direct integration of the three-stage CF model infeasible. In addition, under the environmental conditions evaluated, the CF and Paris law predictions differ only marginally over the period in which O&M actions are typically triggered. Because the investigated O&M strategy intervenes well before the accelerated CF regime emerges, the use of the Paris-law-based formulation in the main analysis yields a conservative rather than optimistic maintenance policy.

Appendix B. Appendix A2: Impact of crack-growth modelling choices on O&M optimisation

To assess influences of the crack-growth modelling choice on the O&M plan, this section evaluates the maintenance schedules derived under both the CF model and the crack-growth model used in the main text. As noted in Appendix A.1, the CF formulation cannot be incorporated directly into the DBN–POMDP framework due to its non-stationary and regime-switching nature. Accordingly, the comparison is performed at the level of the POMDP transition matrices, which encode deterioration progression under each model [161]. The analysis is carried out on a monthly time scale, with the mean wind speed of each month serving as the environmental descriptor. Separate transition matrices are generated using the CF model and the adopted formulation, and an additional CF case at the highest corrosivity C5, as shown in Fig. A3.

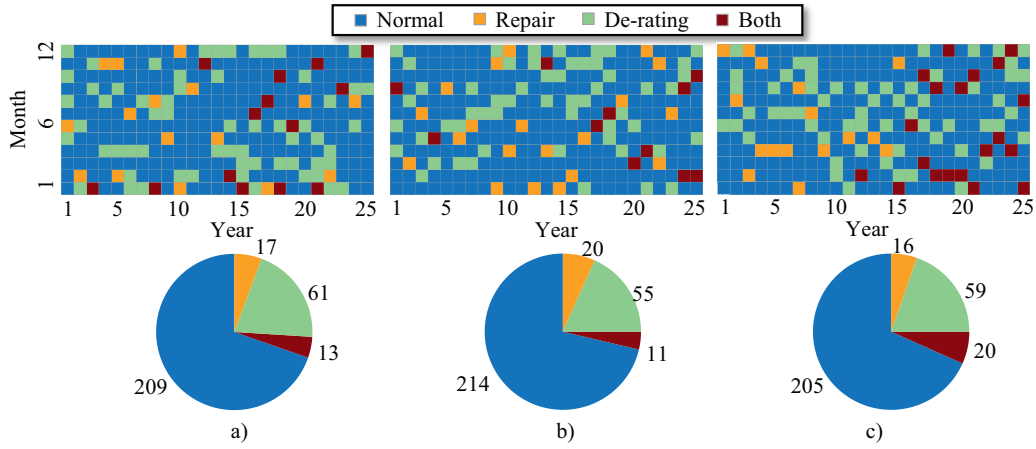

Fig. A3. Effect of crack-growth modelling and corrosivity severity on the resulting O&M schedules: a) adopted model, b) CF model under the same environment, and c) CF model under C5 condition.

From Fig. A3a, b), the crack-growth model adopted in the main analysis leads to a more conservative O&M policy compared with the CF-based transition model under the same environmental conditions. When using the adopted model (Fig. A3a), the FOWT remains in the Normal state for fewer months, while both Repair and De-rating actions are triggered more frequently. The pie chart indicates that only approximately 69% of the monthly decisions correspond to Normal operation, whereas the CF-based model under identical site conditions (Fig. A3b) maintains Normal operation for around 76% of the months. Correspondingly, the shares of Repair and De-rating in Fig. A3a (roughly 13% and 15%) are noticeably higher than those in Fig. A3b (about 9% and 11%). The combined action "Both" also appears more often in Fig. A3a than in Fig. A3b. The results confirm that the crack-growth model used in the main text leads to earlier and more frequent interventions.

In contrast, when corrosion severity reaches the ISO C5 category (Fig. A 3c), the maintenance behaviour changes markedly. Normal operation is reduced to approximately 58% of the months, and both Repair and De-rating account for substantially larger fractions of the decision space (about 18% and 19%, respectively), with an increase in the combined "Both" actions as well. This reflects the rapid deterioration imposed by highly corrosive environments, where the model predicts sustained reliance on De-rating and repeated repairs to maintain structural reliability. Overall, the findings confirm that the deterioration representation used in the main text does not underestimate structural risk; instead, it drives a safety-biased O&M strategy whose superiority remains robust even when CF interactions are considered.

Appendix C. Appendix B: Sensitivity of the discount factor γ

A sensitivity study was conducted to evaluate the influence of the discount factor on the learning dynamics and lifecycle performance of the A3C-based controller. The discount factor was varied over $\gamma \in \{0.98, 0.99, 0.995, 0.999\}$, while all other hyperparameters and stochastic input trajectories remained unchanged. The metric displayed on the left axis of Fig. B1 represents the normalized multi-objective overall performance utility, where higher values indicate superior lifecycle behaviour. The right axis reports the training time required for convergence of the A3C algorithm under each γ setting. As shown in Fig. B1, a discount factor of $\gamma = 0.99$ yields an overall performance of 0.840 with a convergence time of 17.22 h. Decreasing the discount factor to $\gamma = 0.98$ leads to a reduction of overall performance to 0.828 (-1.4% relative to $\gamma = 0.99$) while shortening the training duration to 14.6 h ($\approx 0.85\times$). Increasing the discount factor beyond 0.99 produces only marginal or negative changes in overall performance while substantially increasing training time. For $\gamma = 0.995$, the overall performance reaches 0.841 ($+0.1\%$), whereas the training time increases to 31.2 h ($\approx 1.8\times$ slower). For $\gamma = 0.999$, the overall performance decreases to 0.837 (-0.4%), despite the substantially longer training duration of 48.2 h ($\approx 2.8\times$ slower).

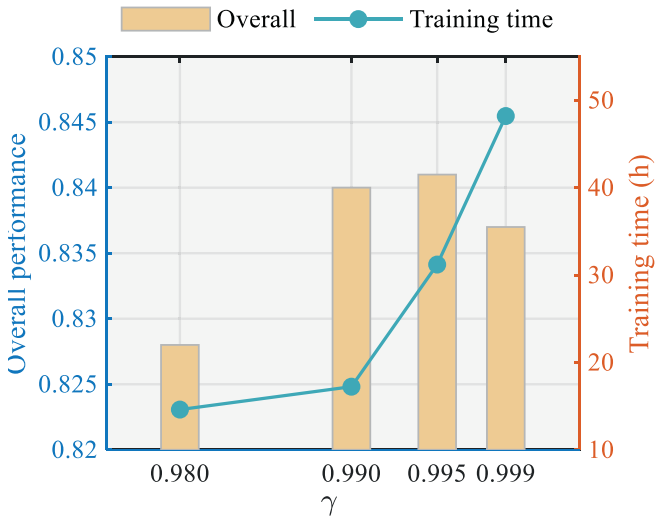

Fig. B1. Influence of the discount factor γ on overall lifecycle performance and training duration

The trend in Fig. B1 indicates that $\gamma = 0.99$ already covers the relevant decision horizon in the FOWT O&M maintenance problem. The marginal increase in overall performance at $\gamma = 0.995$ is statistically negligible but accompanied by a large rise in training time. At $\gamma = 0.999$, performance becomes slightly worse despite an even longer training duration. This behaviour is consistent with established results in reinforcement learning and Markov decision processes. As the discount factor γ approaches 1, the effective planning horizon increases and the Bellman operator becomes a weaker contraction, which is known to slow down value-function convergence, especially in stochastic environments [162,163]. $\gamma = 0.99$ is therefore adopted as the discount factor in this study, offering the best balance between stability, robustness and computational efficiency.

Appendix D. Appendix C: Experimental design and analysis of multi-objective weighting

In the main text, the reward was formulated using equal weights across the four objectives. Earlier work on multi-attribute utility functions coupled with A3C has shown, however, that policy decisions in lifecycle optimisation are sensitive to the preferences embedded in the reward structure [161]. To examine this sensitivity and to assess the relative robustness of OppOM under different decision-making contexts, an additional weight-combination analysis in the section is introduced. Alongside the equal-weight baseline used in the main analysis (Case 0), four further scenarios were constructed to reflect typical stakeholder priorities, favouring asset health, cost, energy, or carbon mitigation. The weight assignments are listed in Table C1.

Table C1
Reward weight schemes for the five preference scenarios.

Item	Scheme	w_h	w_c	w_e	w_{CO2}	Description
0	Balanced	0.25	0.25	0.25	0.25	Neutral configuration
1	Health-prioritized	0.60	0.15	0.15	0.10	Focus on asset integrity
2	Cost-prioritized	0.15	0.60	0.15	0.10	Emphasizes cost efficiency
3	Energy-prioritized	0.15	0.15	0.60	0.10	Maximizes energy yield
4	Carbon-prioritized	0.15	0.15	0.10	0.60	Emphasizes emission reduction

Using the O&M optimisation framework developed in this study, these five weight schemes were evaluated, resulting in eight independent A3C training runs. Fig. C1 compares CBM, OppM and OppOM across the five reward configurations, each representing a distinct preference structure that is likely to arise in practical wind-farm decision making. Fig. C1 illustrates the performance of CBM, OppM, and OppOM across the five reward-weight configurations (Case 0–4), where each case corresponds to a distinct prioritization of turbine health, production, cost, or carbon mitigation.

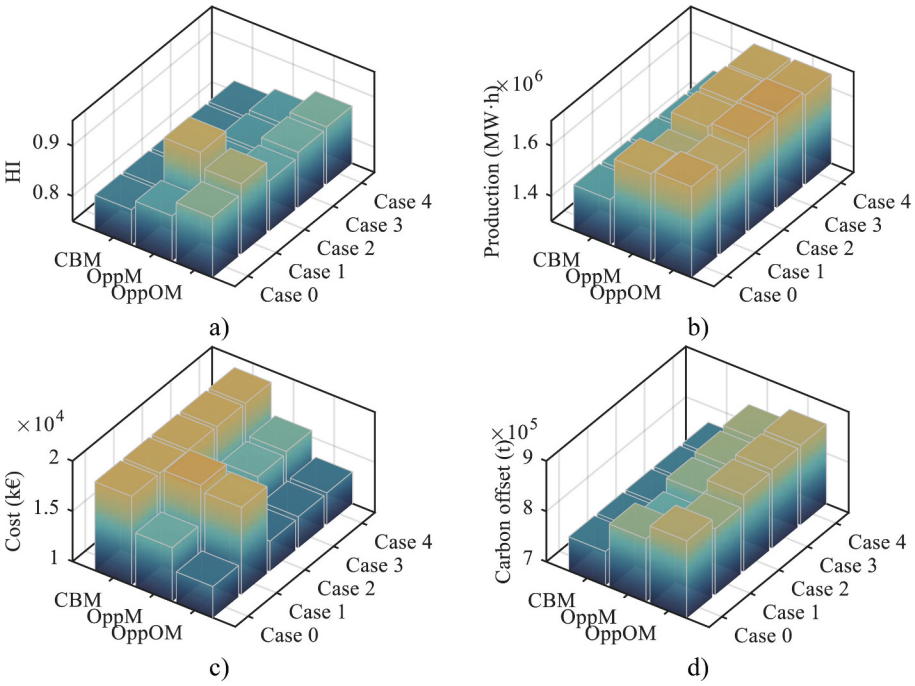

Fig. C1. Sensitivity analysis of CBM, OppM, and OppOM under five reward-weight configurations. a) HI, b) energy production, c) cost, and d) carbon offset.

From Fig. C1 a), OppOM achieves the highest *HI* in four out of the five weight configurations. For example, in the balanced setting (Case 0), *HI* increases from 0.82 (CBM) and 0.84 (OppM) to 0.87 under OppOM, and similarly in the cost-, energy- and carbon-prioritized settings (Cases 2–4), HI improves from 0.834–0.836 (OppM) to 0.85–0.864. The only case in which OppM surpasses OppOM is the health-prioritized configuration (Case 1), where OppM reaches 0.92 while OppOM reaches 0.89. This is attributed to OppM exclusive reliance on component repairs, which provide a direct but costly rise in structural integrity. The accompanying degradation in production, cost and carbon performance (see Fig. C1 b–d) indicates a tendency toward over-maintenance when health becomes the dominant objective. In contrast, OppOM balances selective repairs with de-rating actions, slowing degradation with smaller production and cost penalties and thereby achieving a higher efficiency in health improvement per unit resource expenditure. From Fig. C1b–d), which report total energy production, lifecycle cost and carbon offset respectively, all three metrics show a similar trend across the five weighting scenarios: OppOM consistently outperforms both CBM and OppM. Under the balanced case, production increases from 1.48×10^6MWh (CBM) and 1.65×10^6MWh (OppM) to 1.66×10^6MWh for OppOM; lifecycle cost decreases from 18 832 k€ (CBM) and 15 352 k€ (OppM) to 13 103 k€, and the carbon offset rises from 7.67×10^5t (CBM) and 8.25×10^5t (OppM) to 8.54×10^5t. Comparable margins are observed when cost, energy or carbon is prioritized (Cases 2–4), indicating that OppOM can enhance one objective without substantially compromising the others. In contrast, OppM tends to increase one metric at the expense of at least one other metric depending on the active weighting scheme. For instance, improving HI in Case 1 but worsening production, cost and carbon outcomes. Overall, the relative ranking of the three strategies remains unchanged across all five configurations: OppOM consistently delivers the most balanced and favorable combination of health, production, cost and carbon outcomes. The results confirm that the advantage of OppOM is not tied to a particular reward specification but remains robust under substantially different stakeholder preference structures.

Data availability

Data will be made available on request.

References

[1] Zhang J, et al. Multi-physical driven time-dependent reliability analysis framework for reinforced concrete floating wind turbine foundations considering climate change. Thin-Walled Struct 2025;213:113309.
[2] McMorland J, et al. Operation and maintenance for floating wind turbines: A review. Renew Sust Energ Rev 2022;163:112499.
[3] Jonkman JM. Dynamics modeling and loads analysis of an offshore floating wind turbine. University of Colorado at Boulder; 2007.
[4] Yuan X, et al. Deep analysis of power regulation on fatigue loads and platform motion in floating wind turbines. Ocean Eng 2024;313:119667.
[5] Weller S., et al. Failure implications of different mooring spread and lines. Public Summary Report, Floating Offshore Wind Centre of Excellence (FOW CoE) / ORE Catapult, Report No. PN000584-RPT-006–Rev1, 2024.
[6] Coraddu A, et al. Floating offshore wind turbine mooring line sections health status nowcasting: From supervised shallow to weakly supervised deep learning. Mech Syst Signal Process 2024;216:111446.
[7] Centeno-Telleria M, et al. O&M-aware techno-economic assessment for floating offshore wind farms: A geospatial evaluation off the North Sea and the Iberian Peninsula. Appl Energy 2024;371:123684.
[8] Rowell D, et al. How does the accessibility of floating wind farm sites compare to existing fixed bottom sites? Energies 2022;15(23):8946.
[9] McCoy A, et al. Offshore Wind Market Report. In: Edition. 2024, National Renewable Energy Laboratory (NREL). CO (United States): Golden; 2024.
[10] Stehly T, Duffy P, Mulas Hernando D. Cost of Wind Energy Review. National Renewable Energy Laboratory (NREL): Golden, CO; 2024. Edition. 2024.
[11] McMorland J, et al. Opportunistic maintenance for offshore wind: A review and proposal of future framework. Renew Sust Energ Rev 2023;184:113571.
[12] International Electrotechnical, C., IEC TS 61400-28. Wind energy generation systems - Part 28: Through-life management and life extension of wind power assets. 2025, International Electrotechnical Commission (IEC): Geneva, Switzerland108; 2025.
[13] Gonzalez-Rodriguez AG. Review of offshore wind farm cost components. Energy Sustain Development 2017;37:10–9.
[14] Garcia-Teruel A, et al. Life cycle assessment of floating offshore wind farms: An evaluation of operation and maintenance. Appl Energy 2022;307:118067.
[15] Martin R, et al. Sensitivity analysis of offshore wind farm operation and maintenance cost and availability. Renew Energy 2016;85:1226–36.
[16] Bagheri Nia M, Edalat P. Strategic decision-making in offshore oil and gas platform-to-wind turbine conversion: An integrated analysis of structural

integrity into retrofit lifecycle costs and climate change impacts. Appl Energy 2025;389:125728.
[17] Santos F, Teixeira A, Guedes Soares C. An age-based preventive maintenance for offshore wind turbines. Safety Reliability: Method Appli 2015:1147–55.
[18] Sun Y, et al. Condition-based maintenance for the offshore wind turbine based on long short-term memory network. Proceedings of the institution of mechanical engineers. Part O: J Risk Reliability 2022;236(4):542–53.
[19] Carroll J, McDonald A, McMillan D. Failure rate, repair time and unscheduled O&M cost analysis of offshore wind turbines. Wind Energy 2016;19(6):1107–19.
[20] Li M, Jiang X, Negenborn RR. Opportunistic maintenance for offshore wind farms with multiple-component age-based preventive dispatch. Ocean Eng 2021;231:109062.
[21] Ren Z, et al. Offshore wind turbine operations and maintenance: A state-of-the-art review. Renew Sust Energ Rev 2021;144:110886.
[22] Kang J, Wang Z, Guedes Soares C. Condition-based maintenance for offshore wind turbines based on support vector machine. Energies 2020;13(14):3518.
[23] Oh SY, et al. Condition-based maintenance of wind turbine structures: A state-of-the-art review. Renew Sust Energ Rev 2024;204:114799.
[24] Besnard F, Bertling L. An approach for condition-based maintenance optimization applied to wind turbine blades. IEEE Transact Sustain Energy 2010;1(2):77–83.
[25] Njiri JG, Söffker D. State-of-the-art in wind turbine control: Trends and challenges. Renew Sust Energ Rev 2016;60:377–93.
[26] Dalgic Y, et al. Advanced logistics planning for offshore wind farm operation and maintenance activities. Ocean Eng 2015;101:211–26.
[27] Zhou P, Yin P. An opportunistic condition-based maintenance strategy for offshore wind farm based on predictive analytics. Renew Sust Energ Rev 2019;109:1–9.
[28] Li M, et al. An opportunistic maintenance strategy for offshore wind turbine system considering optimal maintenance intervals of subsystems. Ocean Eng 2020;216:108067.
[29] Kang J, Soares CG. An opportunistic maintenance policy for offshore wind farms. Ocean Eng 2020;216:108075.
[30] Erguido A, et al. After-sales services optimisation through dynamic opportunistic maintenance: a wind energy case study. Proceedings of the institution of mechanical engineers. Part O: J Risk Reliability 2018;232(4):352–67.
[31] Besnard F, et al. An optimization framework for opportunistic maintenance of offshore wind power system. in 2009 IEEE bucharest powertech. IEEE; 2009.
[32] Besnard F, et al. A stochastic model for opportunistic maintenance planning of offshore wind farms. in 2011 IEEE Trondheim PowerTech. IEEE; 2011.
[33] Si G, et al. Maintenance scheduling and vessel routing for offshore wind farms with multiple ports considering day-ahead wind-wave predictions. Appl Energy 2025;379:124915.
[34] Li M, et al. A multi-objective maintenance strategy optimization framework for offshore wind farms considering uncertainty. Appl Energy 2022;321:119284.
[35] Xiang L, et al. Condition monitoring and anomaly detection of wind turbine based on cascaded and bidirectional deep learning networks. Appl Energy 2022;305:117925.
[36] Lee N, Woo J, Kim S. A deep reinforcement learning ensemble for maintenance scheduling in offshore wind farms. Appl Energy 2025;377:124431.
[37] Centeno-Telleria M, et al. Assessing heavy maintenance alternatives for floating offshore wind farms: Towing vs. onsite replacement strategies. Appl Energy 2025;377:124437.
[38] Kennedy K, et al. Genetic optimisation for a stochastic model for opportunistic maintenance planning of offshore wind farms. in 2016 4th International Symposium on Environmental Friendly Energies and Applications (EFEA). IEEE; 2016.
[39] Si G, et al. Holistic opportunistic maintenance scheduling and routing for offshore wind farms. Renew Sust Energ Rev 2025;207:114991.
[40] van Remmerden J, et al. Deep multi-objective reinforcement learning for utility-based infrastructural maintenance optimization. Neural Comput & Applic 2025:1–24.
[41] Cevasco D, Koukoura S, Kolios A. Reliability, availability, maintainability data review for the identification of trends in offshore wind energy applications. Renew Sust Energ Rev 2021;136:110414.
[42] Abdollahzadeh H, Atashgar K, Abbasi M. Multi-objective opportunistic maintenance optimization of a wind farm considering limited number of maintenance groups. Renew Energy 2016;88:247–61.
[43] Valet A, et al. Opportunistic maintenance scheduling with deep reinforcement learning. J Manuf Syst 2022;64:518–34.
[44] Najafi S, Lee C-G. A deep reinforcement learning approach for repair-based maintenance of multi-unit systems using proportional hazards model. Reliab Eng Syst Saf 2023;234:109179.
[45] Schlechtingen M, Santos IF. Wind turbine condition monitoring based on SCADA data using normal behavior models. Part 2: Application examples. Appl Soft Comput 2014;14:447–60.
[46] Dao CD, et al. Integrated condition-based maintenance modelling and optimisation for offshore wind turbines. Wind Energy 2021;24(11):1180–98.
[47] Byon E, Ding Y. Season-dependent condition-based maintenance for a wind turbine using a partially observed Markov decision process. IEEE Trans Power Syst 2010;25(4):1823–34.
[48] Liu C, Hammad A, Itoh Y. Maintenance strategy optimization of bridge decks using genetic algorithm. J Transp Eng 1997;123(2):91–100.
[49] Frangopol DM, Liu M. Bridge network maintenance optimization using stochastic dynamic programming. J Struct Eng 2007;133(12):1772–82.
[50] Liu J, et al. Data fusion for multi-source sensors using GA-PSO-BP neural network. IEEE Trans Intell Transp Syst 2020;22(10):6583–98.
[51] Dong Y, Frangopol DM, Saydam D. Sustainability of highway bridge networks under seismic hazard. J Earthq Eng 2014;18(1):41–66.
[52] Shen C, Jiang B, Yue L. LSTM combined with BIM technology in the management of small and medium-sized span highway concrete beam bridges. Results Eng 2023;20:101539.
[53] Pinciroli L, et al. Optimal operation and maintenance of energy storage systems in grid-connected microgrids by deep reinforcement learning. Appl Energy 2023;352:121947.
[54] Arcieri G, et al. A Comparison of Value-based and Policy-based Reinforcement Learning for Monitoringinformed Railway Maintenance Planning. Struct Health Monit 2023:2023.
[55] Zhou L, Yu J. Resource allocation for high-speed train communication based on deep reinforcement learning. J Phys Conf Ser 2021;1827(1):012184.
[56] Pinciroli L, et al. Deep reinforcement learning based on proximal policy optimization for the maintenance of a wind farm with multiple crews. Energies 2021;14(20):6743.
[57] Wu Y, et al. Reinforcement Learning for Reliable Power Allocation and Load Mitigation in Wind Farm. in 2024 7th International Conference on Renewable Energy and Power Engineering (REPE). IEEE; 2024.
[58] Deng Z, et al. Decentralized yaw optimization for maximizing wind farm production based on deep reinforcement learning. Energy Convers Manag 2023;286:117031.
[59] Didier F, Laghrouche S, Depernet D. Deep Reinforcement Learning-Based Pitch Control for Floating Offshore Wind Turbines. in 2023 9th International Conference on Control, Decision and Information Technologies (CoDIT). IEEE; 2023.
[60] Truong HVA, et al. Active control strategies for system enhancement and load mitigation of floating offshore wind turbines: A review. Renew Sust Energ Rev 2022;170:112958.
[61] Shah KA, et al. A synthesis of feasible control methods for floating offshore wind turbine system dynamics. Renew Sust Energ Rev 2021;151:111525.
[62] Kipchirchir E, et al. Prognostics-based adaptive control strategy for lifetime control of wind turbines. Wind Energy Sci 2023;8(4):575–88.
[63] Pascu V, Kanev S, van Wingerden JW. Adaptive tower damping control for offshore wind turbines. Wind Energy 2017;20(5):765–81.
[64] Capaldo M, Mella P. Damping analysis of Floating Offshore Wind Turbine (FOWT): a new control strategy reducing the platform vibrations. Wind Energy Sci Discussions 2022;2022:1–29.
[65] Galinos C, Larsen TJ, Mirzaei M. Impact on wind turbine loads from different down regulation control strategies. J Phys Conf Ser 2018;1104(1):012019.
[66] Galinos C, Urbán AM, Lio WH. Optimised de-rated wind turbine response and loading through extended controller gain-scheduling. J Phys Conf Ser 2019;1222(1):012020.
[67] Kim S, Kim D, Kim B. Effect of multiple load reduction control systems on the ultimate load and fatigue load of 4 MW class wind turbine. J Renewable Sustain Energy 2020;12(5).
[68] Yao Q, Liu J, Hu Y. Optimized active power dispatching strategy considering fatigue load of wind turbines during de-loading operation. IEEE Access 2019;7:17439–49.
[69] Kipchirchir E, et al. Adaptive robust observer-based control for structural load mitigation and speed regulation in commercial wind turbines. IEEE Access; 2024.
[70] Njiri JG, et al. Consideration of lifetime and fatigue load in wind turbine control. Renew Energy 2019;131:818–28.
[71] Richards PW, Griffith D, Hodges DH. Operating Strategies and Design Recommendations for Mitigating Local Damage Effects in Offshore Turbine Blades. Sandia National Lab.(SNL-NM), Albuquerque, NM (United States); 2014.
[72] Odgaard PF, et al. Optimized control strategy for over loaded offshore wind turbines. Proceedings of Ewea Offshore. 2015.
[73] Pan S, et al. Improved Virtual Inertia Control of Wind Turbine Generators Considering Fatigue Load. in 2023 IEEE 13th International Conference on CYBER Technology in Automation, Control, and Intelligent Systems (CYBER). IEEE; 2023.
[74] van der Hoek D, Kanev S, Engels W. Comparison of down-regulation strategies for wind farm control and their effects on fatigue loads. in 2018 Annual American Control Conference (ACC). IEEE; 2018.
[75] Dimitrov N, Natarajan A. Wind farm set point optimization with surrogate models for load and power output targets. J Phys Conf Ser 2021;2018(1). 012013.
[76] Juangarcia DA, Eguinoa I, Knudsen T. Derating a single wind farm turbine for reducing its wake and fatigue. J Phys Conf Ser 2018;1037(3):032039.
[77] Beganovic N, Njiri JG, Söffker D. Reduction of structural loads in wind turbines based on an adapted control strategy concerning online fatigue damage evaluation models. Energies 2018;11(12):3429.
[78] Chen Z, et al. Joint optimization of opportunistic maintenance and speed control for continuous process manufacturing systems considering stochastic imperfect maintenance. Comput Ind Eng 2024;198:110685.
[79] Santos FP, Teixeira ÂP, Guedes Soares C. Operation and maintenance of floating offshore wind turbines. Floating Offshore Wind Farms 2016:181–93.
[80] Hu L, et al. Short-term prediction of mooring tension for floating offshore wind turbines under typhoon conditions based on the VMD-MI-LSTM method. Renew Sust Energ Rev 2025;216:115606.
[81] Rauf H, Khalid M, Arshad N. Machine learning in state of health and remaining useful life estimation: Theoretical and technological development in battery degradation modelling. Renew Sust Energ Rev 2022;156:111903.
[82] Morato PG, et al. Optimal inspection and maintenance planning for deteriorating structural components through dynamic Bayesian networks and Markov decision processes. Struct Saf 2022;94:102140.

[83] Frangopol DM, Liu M. Maintenance and management of civil infrastructure based on condition, safety, optimization, and life-cycle cost. Struct infrastruct Syst 2019:96–108.
[84] Darmawan MS, Stewart MG. Spatial time-dependent reliability analysis of corroding pretensioned prestressed concrete bridge girders. Struct Saf 2007;29 (1):16–31.
[85] Donahue JR, Lass AB, Burns JT. The interaction of corrosion fatigue and stress-corrosion cracking in a precipitation-hardened martensitic stainless steel. NPJ Materials Degradation 2017;1(1):11.
[86] Le B, Andrews J. Modelling wind turbine degradation and maintenance. Wind Energy 2016;19(4):571–91.
[87] Lee D, Kwon K. Dynamic Bayesian network model for comprehensive risk analysis of fatigue-critical structural details. Reliab Eng Syst Saf 2023;229:108834.
[88] Amzallag C, et al. Standardization of the rainflow counting method for fatigue analysis. Int J Fatigue 1994;16(4):287–93.
[89] Turon A, et al. Simulation of delamination propagation in composites under high-cycle fatigue by means of cohesive-zone models. 2006.
[90] American Bureau S, et al. Fracture Analysis — Guidance Notes (Feb 2022). In: The Society of International Gas Tanker and Terminal Operators (SIGTTO) / EAGLE (as publisher host): London; 2022.
[91] Laitila P, Virtanen K. Improving construction of conditional probability tables for ranked nodes in Bayesian networks. IEEE Trans Knowl Data Eng 2016;28(7): 1691–705.
[92] Zhao Z, Haldar A. Bridge fatigue damage evaluation and updating using non-destructive inspections. Eng Fract Mech 1996;53(5):775–88.
[93] Kurz JH, et al. Reliability considerations of NDT by probability of detection (POD) determination using ultrasound phased array. Eng Fail Anal 2013;35:609–17.
[94] Rudlin J. Multi-channel ultrasonic inspection of a mooring chain for fatigue cracks. in European Conference on Non-Destructive Testing. 2014.
[95] Kurz JH, Dugan S, Juengert A. Reliability considerations of NDT by probability of detection (POD). Determination using ultrasound phased array. Results from a project in frame of the German nuclear safety research program. in 5" t" h European-American workshop on reliability of NDE. Proceedings. 2013.
[96] Kim JW, Choi GB, Lee JM. A POMDP framework for integrated scheduling of infrastructure maintenance and inspection. Comput Chem Eng 2018;112:239–52.
[97] Pineau J, Gordon G, Thrun S. Anytime point-based approximations for large POMDPs. J Artif Intell Res 2006;27:335–80.
[98] Zhang J, et al. Coupling multi-physics models to corrosion fatigue prognosis of high-strength bolts in floating offshore wind turbine towers. Eng Struct 2024;301: 117309.
[99] Ramírez JGR, Sørensen JD. Maintenance Planning of Offshore Wind Turbine using Condition Monitoring Information. in Proceedings of the 28th International Conference on Ocean, Offshore and Arctic Engineering: OMAE2009, May 31-June 5, 2009, Honolulu, Hawaii, USA. American Society of Mechanical Engineers; 2009.
[100] Liu G, et al. Optimum opportunistic maintenance schedule incorporating delay time theory with imperfect maintenance. Reliab Eng Syst Saf 2021;213:107668.
[101] Jensen TN, Knudsen T, Bak T. Fatigue minimising power reference control of a de-rated wind farm. J Phys Conf Ser 2016;753(5):052022.
[102] NREL. A Reference Open Source Controller for Wind Turbines. Available from, https://github.com/NREL/ROSCO; 2024.
[103] Heng J, et al. Influence of Adaptive Controlling Strategies of Floating Offshore Wind Turbine on Corrosion Fatigue Deterioration of Supporting Towers. in International Conference" Coordinating Engineering for Sustainability and Resilience". Springer Nature Switzerland Cham; 2024.
[104] Cheng Y, et al. Fragility and vulnerability development of offshore wind turbines under aero-hydro loadings. Eng Struct 2023;293:116625.
[105] Standard B. Eurocode 3: Design of steel structures-Part 1-9: Fatigue. European Committee for Standardization: Brussels, Belgium; 2005.
[106] AS, D.N.V. Fatigue design of offshore steel structures. Rev3; 2011.
[107] Yang Y, et al. Reviewing the progress of corrosion fatigue research on marine structures. Front Mater 2024;11:1399292.
[108] HDBK M. Nondestructive evaluation system reliability assessment. Department of Defense Handbook7; 2009. p. 15.
[109] Lambert D, Peterson B, Terpenning I. Nondetects, detection limits, and the probability of detection. J Am Stat Assoc 1991;86(414):266–77.
[110] Dai L, Stålhane M, Utne IB. Routing and scheduling of maintenance fleet for offshore wind farms. Wind Eng 2015;39(1):15–30.
[111] Raknes NT, et al. Scheduling of maintenance tasks and routing of a joint vessel fleet for multiple offshore wind farms. J Mar Sci Eng 2017;5(1):11.
[112] Brander M, et al. Scope 2 and market-based accounting-workshop report. Carbon Management 2024;15(1):2324813.
[113] Clauser C, Ewert M. The renewables cost challenge: Levelized cost of geothermal electric energy compared to other sources of primary energy–Review and case study. Renew Sust Energ Rev 2018;82:3683–93.
[114] Eberle S, et al. Multivariate simulation of offshore weather time series: a comparison between markov chain, autoregressive, and long short-term memory models. Wind 2022;2(2):394–414.
[115] Dinwoodie I, Quail F, McMillan D. Analysis of offshore wind turbine operation and maintenance using a novel time domain meteo-ocean modeling approach. In: Turbo Expo: Power for Land, Sea, and Air. American Society of Mechanical Engineers; 2012.
[116] Kijima M. Some results for repairable systems with general repair. J Appl Probab 1989;26(1):89–102.
[117] Veritas DN. Risk based inspection of offshore topsides static mechanical equipment. Standard No. DNV AS. Norway: Høvik; 2010.
[118] Veritas DN. DNV-RP-G101 Risk based inspection of offshore topsides static mechanical equipment. Oslo: DNV; 2010.
[119] Tolsma-de Klerk E. Exploring API 581: Delving into Risk-Based Inspection Calculations. 2025.
[120] Shafiee M, Finkelstein M. An optimal age-based group maintenance policy for multi-unit degrading systems. Reliab Eng Syst Saf 2015;134:230–8.
[121] Dekker R, Wildeman RE, Van der Duyn Schouten FA. A review of multi-component maintenance models with economic dependence. Math Meth Oper Res 1997;45:411–35.
[122] Dinh D-H, Do P, Iung B. Maintenance optimisation for multi-component system with structural dependence: Application to machine tool sub-system. CIRP Ann 2020;69(1):417–20.
[123] Jia Q-S. A structural property of optimal policies for multi-component maintenance problems. IEEE Trans Autom Sci Eng 2010;7(3):677–80.
[124] Leppinen J, et al. An optimization model for determining cost-efficient maintenance policies for multi-component systems with economic and structural dependencies. Omega 2024;130:103162.
[125] Erguido A, et al. A dynamic opportunistic maintenance model to maximize energy-based availability while reducing the life cycle cost of wind farms. Renew Energy 2017;114:843–56.
[126] Nielsen JJ, Sørensen JD. On risk-based operation and maintenance of offshore wind turbine components. Reliab Eng Syst Saf 2011;96(1):218–29.
[127] Gennitsaris S, et al. Integrated LCA and DEA approach for circular economy-driven performance evaluation of wind turbine end-of-life treatment options. Appl Energy 2023;339:120951.
[128] Tang H, Wang H, Li C. Time-varying cost modeling and maintenance strategy optimization of plateau wind turbines considering degradation states. Appl Energy 2025;377:124464.
[129] Sarker BR, Faiz TI. Minimizing maintenance cost for offshore wind turbines following multi-level opportunistic preventive strategy. Renew Energy 2016;85: 104–13.
[130] Tao Z, et al. A novel hierarchical failure analysis approach targeting the operation and maintenance of floating offshore wind turbines. Renew Energy 2025;241: 122267.
[131] Li M, et al. Operation and maintenance management for offshore wind farms integrating inventory control and health information. Renew Energy 2024;231: 120970.
[132] Alves Ribeiro J, et al. Offshore wind turbine tower design and optimization: A review and AI-driven future directions. Appl Energy 2025;397:126294.
[133] Travaglini R, Papi F, Bianchini A. Floating wind farms in sea basins with moderate wind speeds: a critical assessment of the potential of low-specific-power turbines in reducing the LCoE. Renew Sust Energ Rev 2025;222:115990.
[134] Sun Z, You X. Life cycle carbon footprint accounting of an offshore wind farm in Southeast China—Simplified models and carbon benchmarks for typhoons. Appl Energy 2024;355:122267.
[135] Tao L, et al. Bridge Optimal Maintenance Using the Multi-attribute Utility Assessment Method. J Basic Sci Eng 2023;31(5):1278–96.
[136] Mateo JRSC. Multi criteria analysis in the renewable energy industry. Springer Science & Business Media; 2012.
[137] DeMiguel V, Garlappi L, Uppal R. Optimal versus naive diversification: How inefficient is the 1/N portfolio strategy? Rev Financ Stud 2009;22(5):1915–53.
[138] National Renewable Energy, L. Definitions of Levelized Cost of Energy. Electricity | 2022 | Annual Technology Baseline (ATB). 2022.
[139] Zhang N, Si W. Deep reinforcement learning for condition-based maintenance planning of multi-component systems under dependent competing risks. Reliab Eng Syst Saf 2020;203:107094.
[140] Huang R, He H, Gao M. Training-efficient and cost-optimal energy management for fuel cell hybrid electric bus based on a novel distributed deep reinforcement learning framework. Appl Energy 2023;346:121358.
[141] Mnih V, et al. Asynchronous methods for deep reinforcement learning. In: International conference on machine learning. PmLR; 2016.
[142] Sun Y, Yin J. Dynamic condition-based maintenance for shock systems based on damage evolutions using deep reinforcement learning. Reliab Eng Syst Saf 2025; 261:111095.
[143] Grondman I, et al. A survey of actor-critic reinforcement learning: Standard and natural policy gradients. IEEE Transact Syst 2012;42(6):1291–307. Man, and Cybernetics, part C (applications and reviews).
[144] Guo Y, et al. Optimal dynamic thermal management for data center via soft actor-critic algorithm with dynamic control interval and combined-value state space. Appl Energy 2024;373:123815.
[145] Nahhas A, Kharitonov A, Turowski K. Deep reinforcement learning techniques for solving hybrid flow shop scheduling problems: Proximal policy optimization (PPO) and asynchronous advantage actor-critic (A3C). 2022.
[146] Chen M, et al. Intelligent resource allocation management for vehicles network: An A3C learning approach. Comput Commun 2020;151:485–94.
[147] McAuliffe J, et al. Corrosion fatigue analysis of NREL's 15-MW offshore wind turbine with time-varying stress concentration factors. J Phys Conf Ser 2024;2767 (6):062023.
[148] Allen C, et al. Definition of the UMaine VolturnUS-S reference platform developed for the IEA wind 15-megawatt offshore reference wind turbine. National Renewable Energy Lab.(NREL), Golden, CO (United States); Univ; 2020.
[149] National Renewable Energy Laboratory (NREL). OpenFAST, version 3.6.0, open-source wind turbine simulation software. GitHub repository. https://github.com/OpenFAST/OpenFAST.

[150] Rinker J, et al. Comparison of loads from HAWC2 and OpenFAST for the IEA Wind 15 MW Reference Wind Turbine. Journal of Physics: Conference Series 2020;1618(5):052052.
[151] Zhong W, et al. Comparison study on mooring line models for hydrodynamic performances of floating offshore wind turbines. Ocean Eng 2024;296:117083.
[152] NDBC, CAPE ELIZABETH. 45NM NW of Aberdeen, WA. Available from: https://www.ndbc.noaa.gov/station_page.php?station=46041; 2019.
[153] Zhu F, et al. Time-domain fatigue reliability analysis for floating offshore wind turbine substructures using coupled nonlinear aero-hydro-servo-elastic simulations. Eng Struct 2024;318:118759.
[154] Glorot X, Bengio Y. Understanding the difficulty of training deep feedforward neural networks. in Proceedings of the thirteenth international conference on artificial intelligence and statistics. JMLR Workshop and Conference Proceedings; 2010.
[155] Jing Q, et al. Intelligent e-maintenance with preference-based decision making using A3C reinforcement learning. Eng Struct 2026;346:121636.
[156] Liu D, et al. Deep reinforcement learning for real-time economic energy management of microgrid system considering uncertainties. Front Energy Res 2023;11:1163053.
[157] Alabi TM, et al. Automated deep reinforcement learning for real-time scheduling strategy of multi-energy system integrated with post-carbon and direct-air carbon captured system. Appl Energy 2023;333:120633.
[158] Standardization, I.O.F. Corrosion of metals and alloys—Corrosivity of atmospheres—Classification, determination and estimation (ISO 9223:2012). Switzerland: ISO: Geneva; 2012.
[159] Ge B, Kim S. Probabilistic service life prediction updating with inspection information for RC structures subjected to coupled corrosion and fatigue. Eng Struct 2021;238:112260.
[160] Murphy KP. Dynamic bayesian networks: representation, inference and learning. Berkeley: University of California; 2002.
[161] Jing Q, et al. Intelligent e-Maintenance for long-span bridges with preference-based decision making using A3C reinforcement learning. Eng Struct 2026;346:121636.
[162] François-Lavet V, Fonteneau R, Ernst D. How to discount deep reinforcement learning: Towards new dynamic strategies. arXiv preprint arXiv:1512.02011. 2015.
[163] Majid AY, et al. Deep reinforcement learning versus evolution strategies: A comparative survey. IEEE Transact Neural Net Learning Syst 2023;35(9):11939–57.